NORSAR

ROYAL NORWEGIAN COUNCIL FOR SCIENTIFIC AND INDUSTRIAL RESEARCH

(1)

Norsar Scientific Report No. 2-83/84

SEMIANNUAL TECHNICAL SUMMARY
1 October 1983 - 31 March 1984

Linda Tronrud (ed.)

Kjeller, May 1984

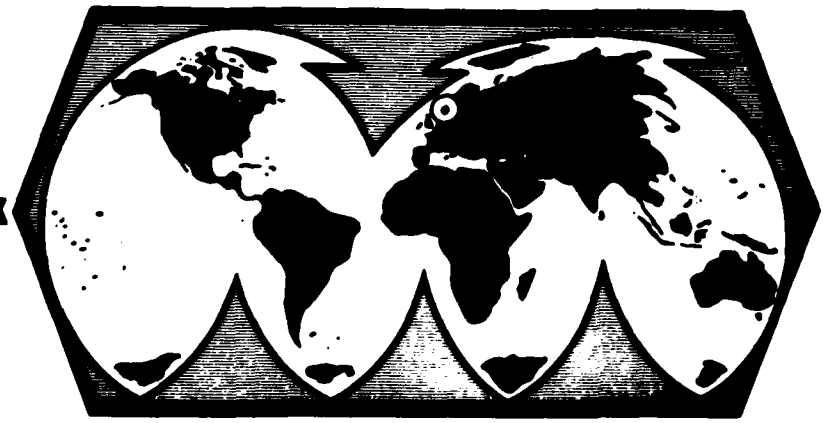

REPORT DOCUMENTATION PAGE

READ INSTRUCTIONS BEFORE COMPLETING FORM

1. REPORT NUMBER	2. GOVT ACCESSION NO. AD-A146778 / 3. RECIPIENT'S CATALOG NUMBER
4. TITLE (and Subtitle) SEMIANNUAL TECHNICAL SUMMARY 1 October 1983 - 31 March 1984	5. TYPE OF REPORT & PERIOD COVERED 1 Oct 83 - 31 Mar 84
	6. PERFORMING ORG. REPORT NUMBER Sci. Report a/83-84
7. AUTHOR(s) L.B. Tronrud (ed.)	8. CONTRACT OR GRANT NUMBER(s)
9. PERFORMING ORGANIZATION NAME AND ADDRESS NTNF/NORSAR Post Box 51 N-2007 Kjeller, Norway	10. PROGRAM ELEMENT, PROJECT, TASK AREA & WORK UNIT NUMBERS NORSAR Phase 3
11. CONTROLLING OFFICE NAME AND ADDRESS AFTAC/HQ/TGX Patrick AFB FL 32925 USA	12. REPORT DATE May 1984
	13. NUMBER OF PAGES 76
14. MONITORING AGENCY NAME & ADDRESS (if different from Controlling Office)	15. SECURITY CLASS. (of this report)
	15a. DECLASSIFICATION/DOWNGRADING SCHEDULE

16. DISTRIBUTION STATEMENT (of this Report)

APPROVED FOR PUBLIC RELEASE; DISTRIBUTION UNLIMITED.

17. DISTRIBUTION STATEMENT (of the abstract entered in Block 20, if different from Report)

18. SUPPLEMENTARY NOTES

19. KEY WORDS (Continue on reverse side if necessary and identify by block number)

20. ABSTRACT (Continue on reverse side if necessary and identify by block number)

This report describes the operation, maintenance and research activities at the Norwegian Seismic Array (NORSAR) for the period 1 October 1983 to 31 March 1984.

DD FORM 1 JAN 73 1473 EDITION OF 1 NOV 65 IS OBSOLETE

The uptime of the NORSAR online detection processor system has averaged 95.6 as compared to 98.8 for the previous period. Most of the longer down periods were caused by a faulty alarm system. A total of 1698 events were reported in this period, giving a daily average of 9.3 events. The number of reported events per month varied from 355 in March to 189 in November. There have been some difficulties with the communications lines, especially the 03C line, which has had power outages due to damaged power lines.

During this reporting period the replacement of the old IBM processing system has been completed. The newest addition was a system printer replacing two system printers in the old computer system. A new graphic software package, GPGS, was installed during this reporting period to increase flexibility and quality of graphic representation at NORSAR.

Section V describes improvements, modifications and maintenance activity in connection with the NORSAR field instrumentation.

The research activity is briefly described in Section VII. Subsection 1 discusses magnitudes, seismicity and earthquake detectability using a global network. Subsection 2 presents a study on observation and modelling of regional phases recorded at NORSAR. Subsection 3 discusses the determination of radiated seismic energy and related source parameters, while subsection 4 presents Fennoscandian seismicity, 1980-84. A source parameter analysis of the 8 March 1983 Stord earthquake is presented in Subsection 5; Subsection 6 reports on an affordable, interactive and mobile seismic array. A preliminary analysis of multichannel seismic refraction data from the FRAM IV ice-drift station experiment is presented in subsection 7. Subsection 8 gives some details on vertical and three-component instrument field experiments performed in 1983 in connection with the new regional array.

AFTAC Project Authorization No.	:	T/4141/B/PMP
ARPA Order No.	:	1483
Program Code No.	:	0F10
Name of Contractor	:	Royal Norwegian Council for Scientific and Industrial Research
Effective Date of Contract	:	1 October 1983
Contract Expiration Date	:	30 September 1984
Project Manager	:	Frode Ringdal (02) 71 69 15
Title of Work	:	The Norwegian Seismic Array (NORSAR) Phase 3
Amount of Contract	:	$796.000
Contract Period Covered by the Report	:	1 October 1983 - 31 March 1984

The views and conclusions contained in this document are those of the authors and should not be interpreted as necessarily representing the official policies, either expressed or implied, of the Defense Advanced Research Projects Agency, the Air Force Technical Applications Center, or the U.S. Government.

This research was supported by the Advanced Research Projects Agency of the Department of Defense and was monitored by AFTAC, Patrick AFB FL 32925, under contract no. F08606-84-C-0002.

NORSAR Contribution No. 345

TABLE OF CONTENTS

I. SUMMARY

This report describes the operation, maintenance and research activities at the Norwegian Seismic Array (NORSAR) for the period 1 October 1983 to 31 March 1984.

The uptime of the NORSAR online detection processor system has averaged 95.6 as compared to 98.8 for the previous period. Most of the longer down periods were caused by a faulty alarm system. A total of 1698 events were reported in this period, giving a daily average of 9.3 events. The number of reported events per month varied from 355 in March to 189 in November. There have been some difficulties with the communications lines, especially the 03C line, which has had power outages due to damaged power lines.

During this reporting period the replacement of the old IBM processing system has been completed. The newest addition was a system printer replacing two system printers in the old computer system. A new graphic software package, GPGS, was installed during this reporting period to increase flexibility and quality of graphic representation at NORSAR.

Section V describes improvements, modifications and maintenance activity in connection with the NORSAR field instrumentation.

The research activity is briefly described in Section VII. Subsection 1 discusses magnitudes, seismicity and earthquake detectability using a global network. Subsection 2 presents a study on observation and modelling of regional phases recorded at NORSAR. Subsection 3 discusses the determination of radiated seismic energy and related source parameters, while subsection 4 presents Fennoscandian seismicity, 1980-84. A source parameter analysis of the 8 March 1983 Stord earthquake is presented in Subsection 5; Subsection 6 reports on an affordable, interactive and mobile seismic array. A preliminary analysis of multichannel seismic refraction data from the FRAM IV ice-drift station experiment is presented in subsection 7. Subsection 8 gives some details on vertical and three-component instrument field experiments performed in 1983 in connection with the new regional array.

II. OPERATION OF ALL SYSTEMS

II.1 Detection Processor (DP) Operation

There have been 130 breaks in the otherwise continuous operation of the NORSAR online system within the current 6-month reporting interval. Most of the long down periods that lasted for hours were caused by the alarm sender not operating correctly, thus giving no alarm. This unit will now be replaced. The uptime percentage for the period is 95.6 as compared to 98.8 for the previous period.

Fig. II.1.1 and the accompanying Table II.1.1 both show the daily DP downtime for the days between 1 October 1983 and 31 March 1984. The monthly recording times and percentages are given in Table II.1.2.

The breaks can be grouped as follows:

a)	Modcomp failure	70
b)	Stops related to possible program errors	23
c)	Maintenance stops	10
d)	Power jumps and breaks	3
e)	Stops related to system operation	1
f)	TOD error correction	21
g)	Communication lines	2

The total downtime for the period was 195 hours and 7 minutes. The mean-time-between-failures (MTBF) was 1.4 days as compared with 1.3 days for the previous period.

J. Torstveit

LIST OF BREAKS IN DP PROCESSING THE LAST HALF-YEAR

DAY	START		STOP		COMMENTS.....
279	7	4	7	5	RESTART MODCOMP
280	7	1	7	5	TOD CORRECTION
284	8	23	8	24	RESTART MODCOMP
284	8	27	8	28	RESTART MODCOMP
284	13	50	13	51	RESTART MODCOMP
284	13	54	13	55	RESTART MODCOMP
284	14	22	14	23	RESTART MODCOMP
286	7	8	10	8	CE WORK (DISC)
287	10	25	10	26	RESTART MODCOMP
287	10	33	10	34	RESTART MODCOMP
287	13	44	14	7	MODCOMP FAILURE
289	0	26	3	40	MODCOMP FAILURE
289	12	22	12	52	MODCOMP FAILURE
289	14	34	15	5	MODCOMP FAILURE
289	23	14	23	46	MODCOMP FAILURE
292	12	27	12	28	SYSTEN ERROR
293	14	32	22	11	MODCOMP FAILURE
293	22	22	22	26	SYSTER ERROR
293	23	22	24	0	MODCOMP FAILURE
294	0	0	4	43	MODCOMP FAILURE
294	5	3	7	39	MODCOMP FAILURE
308	7	3	7	5	MODCOMP FAILURE
309	11	59	23	52	MODCOMP FAILURE
312	6	43	7	5	MODCOMP FAILURE
312	7	31	10	26	MODCOMP FAILURE
314	7	20	7	23	MODCOMP FAILURE
321	7	13	7	14	TOD CORRECTION
322	8	25	8	26	MODCOMP FAILURE
322	14	17	17	23	MODCOMP FAILURE
325	7	19	7	23	TOD CORRECTION
334	15	18	15	19	SYSTEM
334	19	10	19	11	SYSTEM
335	17	43	17	44	SYSTEM FAILURE
336	11	46	11	47	SYSTEM FAILURE
339	8	28	9	29	CE TEST MODEM,2701
339	8	53	9	49	SYSTEM FAILURE
339	11	57	11	58	SYSTEM FAILIRE
340	5	8	9	23	MODCOMP FAILURE
340	10	16	10	23	CE TEST 2701
340	15	50	15	51	SYSTEM FAILURE
342	7	4	7	8	TOD CORRECTION
346	10	0	14	27	POWER BREAK
347	7	9	7	10	TOD CORRECTION
347	12	38	13	22	MODCOMP FAILURE
348	8	8	9	2	IBM CE WORK 2701
349	9	31	9	40	IBM CE WORK 2701
349	13	49	13	52	IBM CE WORK 2701
350	13	8	13	24	IBM CE WORK 2701
352	17	58	18	0	SYSTEM FAILURE
353	1	7	7	4	MODCOMP FAILURE
353	8	32	14	58	MODCOMP POWER FAILURE
353	20	59	21	1	SYSTEM FAILURE
354	7	32	7	34	SYSTEM FAILURE
354	7	37	7	39	SYSTEM FAILURE
355	7	10	7	12	TOD CORRECTION
355	14	20	14	38	SYSTEM FAILURE
355	15	6	24	0	DP SOFTWARE
356	0	0	7	25	DP SOFTWARE
359	10	44	14	25	OPER
361	7	1	7	3	TOD CORRECTION
361	10	4	10	5	SYSTEM FAILURE
362	9	19	11	19	MODCOMP FAILURE
365	23	9	24	0	POWER BREAK
1	0	0	1	5	POWER FAILURE
1	11	30	13	10	SYSTEM WORK
3	7	1	7	3	TOD CORRECTION
3	12	30	12	37	MODCOMP FAILURE
3	13	46	14	58	MODCOMP FAILURE
3	16	8	17	45	MODCOMP FAILURE
5	3	49	8	25	MODCOMP FAILURE
9	7	15	7	16	TOD CORRECTION
12	9	23	10	36	CE WORK TOD MOVED

Table II.1.1 Daily DP downtime in the period 1 Oct 83 - 31 Mar 84. (Page 1 of 2)

LIST OF BREAKS IN DP PROCESSING THE LAST HALF-YEAR

DAY	START		STOP		COMMENTS.....
13	7	8	7	10	TOD CORRECTION
18	7	5	7	8	TOD CORRECTION
18	9	19	10	30	MODCOMP TEST
18	13	22	14	15	MODCOMP TEST
19	13	40	13	57	POWER BREAKE
27	7	11	7	39	SYSTEM FAILURE
33	13	20	14	28	CE WORK MODCOMP
34	9	8	10	50	MODCOMP FAILURE
34	11	27	13	17	MODCOMP FAILURE
37	7	2	7	3	TOD CORRECTION
37	15	3	15	5	MODCOMP FAILURE
38	8	7	9	1	CE INST. CHANGE
41	14	52	14	53	MODCOMP FAILURE
44	7	44	7	46	TOD CORRECTION
44	9	10	10	0	LINE FAILURE
44	14	15	14	45	MODCOMP FAILURE
45	11	35	12	9	MODCOMP FAILURE
45	13	17	13	45	MODCOMP FAILURE
45	15	2	15	15	MODCOMP FAILURE
45	15	26	16	50	MODCOMP FAILURE
45	18	8	20	38	MODCOMP FAILURE
47	6	45	7	28	MODCOMP FAILURE
48	7	55	10	13	MODCOMP FAILURE
48	12	8	12	38	MODCOMP FAILURE
53	6	51	6	52	TOD CORRECTION
53	7	3	7	4	TOD CORRECTION
54	7	4	7	5	SYSTEM FAILURE
55	9	52	9	53	SYSTEM FAILURE
56	8	57	11	4	MODCOMP FAILURE
56	13	41	17	45	MODCOMP FAILURE
56	17	50	17	58	MODCOMP FAILURE
56	18	23	24	0	MODCOMP FAILURE
57	0	0	15	54	MODCOMP FAILURE
57	20	19	24	0	MODCOMP FAILURE
58	0	0	6	45	MODCOMP FAILURE
58	7	54	7	56	MODCOMP FAILURE
59	7	2	7	3	TOD CORRECTION
59	15	35	15	41	MODCOMP FAILURE
59	20	58	21	43	MODCOMP FAILURE
62	15	15	15	45	MODCOMP FAILURE
62	17	39	18	15	MODCOMP FAILURE
65	11	51	11	52	TOD CORRECTION
66	7	56	7	57	TOD CORRECTION
66	9	10	10	14	MODCOMP FAILURE
67	9	1	10	23	MODCOMP FAILURE
67	12	52	13	10	MODCOMP FAILURE
67	18	5	19	31	MODCOMP FAILURE
69	19	53	20	18	MODCOMP FAILURE
70	8	24	9	4	MODCOMP FAILURE
72	11	44	12	19	MODCOMP FAILURE
73	3	3	6	49	MODCOMP FAILURE
73	11	9	11	47	MODCOMP FAILURE
73	14	19	14	34	MODCOMP FAILURE
74	12	36	12	38	SYSTEM WORK
79	7	3	7	4	TOD CORRECTION
79	7	15	7	18	TOD CORRECTION
79	11	5	11	9	SYSTEM WORK
80	14	27	14	30	SYSTEM WORK
82	14	43	15	18	MODCOMP FAILURE
84	15	36	24	0	MODCOMP FAILURE
85	0	0	13	34	MODCOMP FAILURE
86	6	2	6	5	TOD CORRECTION
87	7	35	7	37	LINES OUT OF SYNC
90	7	57	7	59	MODCOMP FAILURE

Table II.1.1 (page 2 of 2)

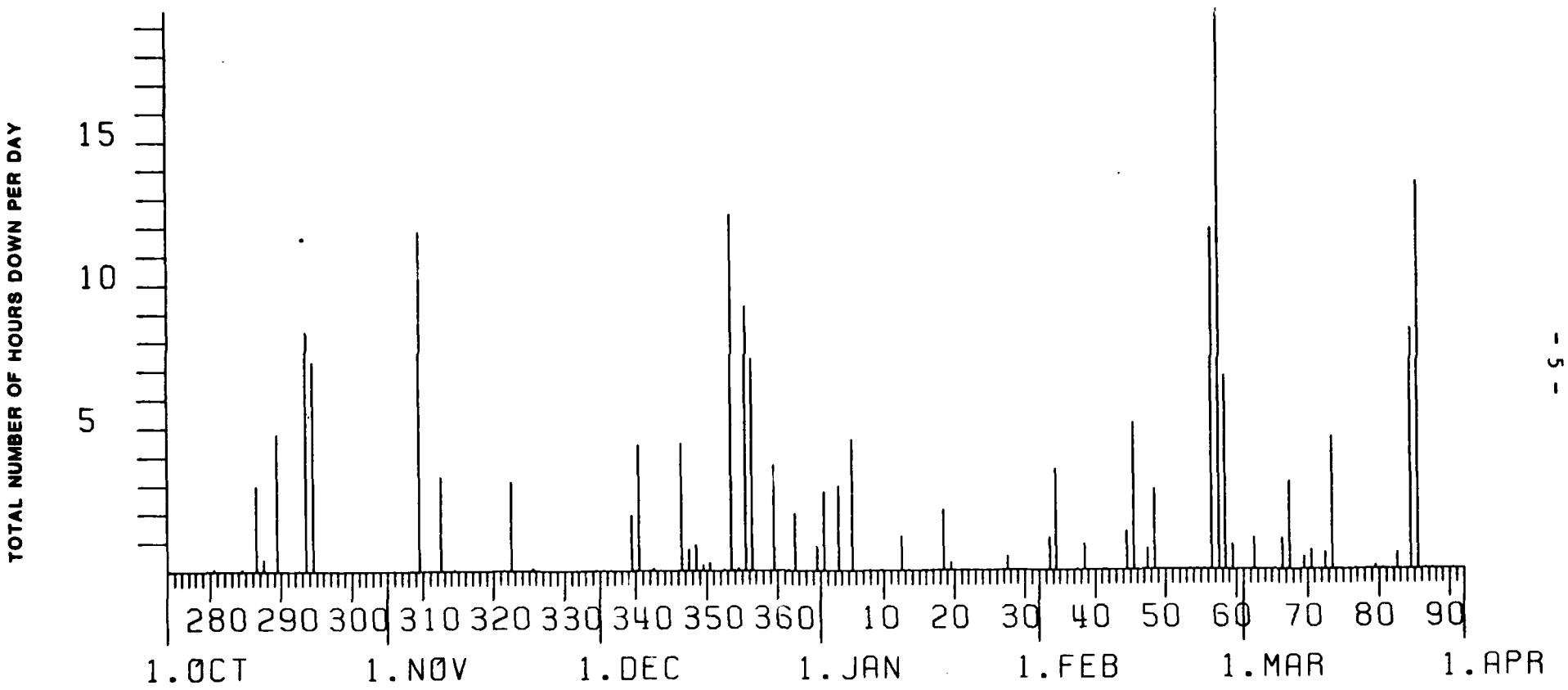

Fig. II.1.1 Detection Processor downtime in the period 1 Oct 1983 - 31 Mar 1984.

Month	DP Uptime (hrs)	DP Uptime (%)	No. of DP Breaks	No. of Days with Breaks	DP MTBF* (days)
Oct	719.97	96.8	20	9	1.4
Nov	701.53	97.7	11	8	2.4
Dec	695.25	93.4	30	19	0.9
Jan	729.57	98.1	14	9	2.0
Feb	641.12	92.1	31	16	0.8
Mar	709.52	95.6	24	17	1.2
	4196.96	95.6	130	78	1.4

*Mean-time-between-failures = (Total uptime/No. of up intervals)

TABLE II.1.2

Online System Performance
1 October 1983 - 31 March 1984

II.2 Array Communication

Table II.2.1 reflects the performance of the communications system throughout the reporting period. Also this report indicates high figures, ref. Table II.2.1. 03C has been affected by power outages caused by damaged power lines; 04C due to lack of power caused by faulty battery charger. 06C communication line is still being used in connection with NORESS. Otherwise the communications systems have been most reliable.

Summary

Oct: 03C was affected four times (5,6,21 and 28 Oct) by trees breaking the power line in connection with strong wind in the area.
04C was down between 6 and 11 Oct due to a faulty battery charger.
The original 06C line still used for transfer of NORESS data.

Nov: Again 03C lost power due to damaged power line (4, 6 and 20 Nov), and remained down throughout the month. The reason for these repeated incidents has connection with the new landowner, who is not fully aware of his responsibility for cutting the trees near the power line.

Dec: This month we had some synchronizing problems with the 02C comm. system.
03C was back in operation (23 Dec) after loss of power (20 Nov).
The modem loop facility (01B) failed in Dec due to a faulty separation filter (AHS-card).

Jan: In January, between 9 and 18, "cross-talk" caused a few problems with the 03C comm. system.
The reliability of the remaining systems was high.

Feb: In February we had reason to believe that the 03C comm. system caused problems when the communications processor (MODCOMP) tried to resynchronize the comm. lines. The processor stopped quite often. The CTV modem digital loop (C-loop) did not function. In order to avoid too many

MODCOMP stops during night hours and still have the possibility to observe the 03C comm. system's effect on the MODCOMP, the subarray was masked.

Mar: 03C remained masked and the comm. line turned off most of the period, apart from during ordinary working hours when the system quite frequently was switched back for observation purposes. Also during periods with the comm. system turned off, a number of MODCOMP stops occurred. From the first period with MODCOMP stops, the situation obviously changed when the 03C comm. line was turned off. 30 Mar the subarray was visited, and among the tasks to be carried out was modem and comm. system checks. Although no action was taken by NTA until then, the comm. system, including the digital loop (C-loop) feature was found to be operating. The subarray was still masked by the end of March.

Table II.2.2 indicates the distribution of outages with respect to the individual subarrays.

Miscellaneous

During the reporting period we have also observed the NORESS and 02B (telemetry) channels. Sometimes it has been difficult to decide whether transmission media or irregularities related to seismometers/amplifiers/cables have caused outages/reduced performance. NORESS channels 01-08 were down 24 hours from 17 Oct. Improper line conditions caused outage of all NORESS channels between 11 and 18 November.

In order to improve line conditions, NMC-designed equalizers were connected 21 November.

O.A. Hansen

Sub-Array	OCT 83 (4) (3-30.10)	NOV 83 (5) (31.10-4.11)	DEC 83 (4) (5.12-1.1.84)	JAN 84 (4) (2-29.1)	FEB 84 (4) (30.1-4.3)	MAR 84 (4) (5.3-1.4)	AVERAGE ½ YEAR
01A	0.004	0.006	0.04	0.003	0.001	0.002	0.009
01B	0.003	0.003	0.03	0.003	0.005	0.001	0.007
02B	0.004	0.009	0.02	0.003	0.005	0.001	0.006
02C	0.004	0.024	3.13	0.002	0.0006	0.001	0.527
03C	* 15.1	* 58.9	* 66.6	0.006	* 27.63	* 85.1	* 42.20
04C	* 15.6	0.004	0.002	0.003	0.001	0.002	2.60
06C	*100.0	*100.0	*100.0	*100.0	*100.0	*100.0	*100.0
AVER	18.67	22.71	24.26	14.29	18.23	26.44	20.76
LESS	03C,04C 06C	03C,06C	03C,06C	06C	03C,06C	03C,06C	03C,06C
	0.004	0.009	0.64	0.003	0.001	0.001	0.63

* See item II.2 regarding figures with asterisks.

TABLE II.2.1

Communications performance. Figures in per cent based on total transmitted frames/week (1.2096×10^7)
(3 October 1983 - 31 March 1984)

Week/ Year	Subarray/per cent outage						
	01A	01B	02B	02C	03C	04C	06C
40/83	0.002	0.002	0.002	0.006	12.5	62.5	100.0
41	0.008	0.006	0.007	0.008	0.007	0.007	100.0
42	0.001	0.007	0.007	0.001	0.001	0.008	100.0
43	0.005	0.006	0.006	0.007	39.3	0.005	100.0
44	0.009	0.007	0.037	0.007	28.6	0.01	100.0
45	-	-	-	-	64.3	-	100.0
46	0.001	0.0005	0.0005	0.0006	1.79	0.005	100.0
47	0.014	0.003	0.004	0.11	100.0	0.004	100.0
48	0.005	0.004	0.004	0.005	100.0	0.006	100.0
49	0.0006	0.0004	0.004	12.5	100.0	0.0006	100.0
50	0.003	0.03	0.002	0.013	100.0	0.003	100.0
51	0.010	0.09	0.001	0.001	66.1	0.002	100.0
52/83/84	0.004	0.004	0.004	0.004	0.004	0.004	100.0
1	0.012	0.011	0.011	0.003	0.012	0.009	100.0
2	0.001	0.001	0.001	0.001	0.012	0.001	100.0
3	0.0001	0.0001	-	0.0002	0.0001	0.0002	100.0
4	0.0002	0.0002	0.0002	0.0003	0.0001	0.0002	100.0
5	-	-	-	-	-	-	100.0
6	0.0004	0.0004	0.0003	0.0003	0.0003	0.0004	100.0
7	0.0003	0.0002	0.0002	0.0002	79.2	0.001	100.0
8	0.001	0.0002	0.0003	0.0004	17.9	0.001	100.0
9	0.002	0.002	0.002	0.002	79.4	0.003	100.0
10	0.002	0.002	0.002	0.002	100.0	0.002	100.0
11	0.00003	0.00003	0.00006	0.002	100.0	0.002	100.0
12	0.002	0.002	0.002	0.002	92.2	0.003	100.0
13	0.003	0.002	0.003	0.002	68.6	0.002	100.0

TABLE II.2.2

Subarray/per cent outage
1 October 1983 - 31 March 1984

III. ARRAY PERFORMANCE

III.1 Event Processor Operation

In Table III.1 some monthly statistics of the Event Processor operation are given:

	Teleseismic	Core Phases	Sum	Daily
Oct 83	193	31	224	7.2
Nov 83	189	39	228	7.6
Dec 83	230	46	276	8.9
Jan 84	262	34	296	9.5
Feb 84	235	39	274	9.4
Mar 84	355	45	400	12.9
	1464	234	1698	9.3

TABLE III.1

B. Kr. Hokland

IV. IMPROVEMENTS AND MODIFICATIONS

NORSAR on-line system using 4331/4341 and MODCOMP Classic

We refer to the detection processor operation statistics for details on system performance.

During this reporting period we have finished the replacement of the old IBM processing system. The latest replacement was a new system printer instead of two system printers from the old computer system.

The main result from NORSAR Data Processing Center and many of the scientists' programs is graphic representation of data. The quality of these plots and the flexibility for programmers in making plots on different devices has not been good enough. During the previous reporting period we installed a VERSATEC raster plotter which has been running very well, and during this period we have installed a new graphic software package called GPGS. The package gives the research people more assistance for graphic representation, easier programming and more flexibility in the programs.

The uptime for the processing system has been slightly lower than usual during the past six months. We have found three main reasons for the downtime, and we list them below:

- error in the alarm system
- error in MODCOMP line interface against SLEM
- continued problems with the 2701 communication processor unit.

An error in the alarm system has resulted in stops up to 20 hours in the weekend without any message to the operating staff. The alarm system is soon to be replaced.

An error in the MODCOMP line interface has resulted in occasional stops of the MODCOMP system. This error has now been located and corrected.

There are still problems with the old communication unit (2701) which is placed between the MODCOMP and the online processor. A consultant has been hired to make a new interface called 1950 between these two systems. Unfortunately, the progress is slow and the implementation is still not completed.

The rest of the processing system has been running satisfactorily and no software or hardware stops have been observed.

The daily procedure at the computer center has now been changes in order to meet the request for telex with bulletins as early as possible. The operator arrives at eight a.m. and the telex is prepared and transmitted before nine o'clock local time.

System group
R. Paulsen

V. MAINTENANCE ACTIVITIES

Activities in the field and at the maintenance center

As indicated by Table V.1 subarray visits in connection with corrective/ preventive maintenance have been limited to: RA-5 replacements (5), SLEM adjustments (3), LP seismometer adjustments (1), AHS-card replacement (3), RCD replacement (1), Well Head Vault drainage (1), power outage with SA visits (3), battery charger replacement (1) and cable replacement/repair (1).

Improvements and modifications

Reference is made to Table V.2 indicating the status of the SP instruments of the NORSAR array. No changes have been made with regard to the provisional NORESS configuration since the last report. In the NORSAR array, wind measuring equipment has been removed from channel 03 and 05 at the subarray 01A, and channels back to normal status.

Array status

As of 31 March 1984 the following channels deviated from tolerances: 01B01; 03C03, 08; 06C (not used).

01A 01 8 Hz filter
02 -"- , 60 m hole
04 Attenuated 30 dB.

O.A. Hansen

SA/ Area	Task	Date
NORESS	NMC manager (P.W. Larsen) took part in geological surveys on different sites in cooperation with NORSAR-engaged consultants (incl. drilling to rock surface). Marking of cable trenches also carried out. Otherwise several meetings with consultant and the landowners.	Oct 11 days
02B	RA-5 ampl. replaced on SP 00, 03 and 04	3 Oct
04C	Remote Centering Device (RCD) Free Period EW Seism. replaced	4 Oct
03C	Separation filter (AHS-card) replaced in modem	5 Oct
02C	RA-5 ampl. replaced on SP02. Well Head Vault and borehole drained	6 Oct
02B	RA-5 ampl. replaced on SP01	7 Oct
03C	Power outage called for action	7 Oct
04C	Battery charger replaced	11 Oct
02C	Borehole SP02 drained	14 Oct
01B	RA-5 ampl. replaced SP05	20 Oct
03C	Power outage	21 Oct
01B	Cable fault SP02 located and mended	21 Oct
NORESS	Several meetings between landowners (A/S Borregård), the consultant (Østlandkonsult) and NMC (P.W. Larsen) were held. Final marking of cable trenches. Ready for wood clearing.	Nov
NORESS/ NDPC	Line equalizers for improvement of NORESS lines designed and integrated in the remaining NORESS equipment (F.M. discriminator, etc.) at the NDPC.	Nov

TABLE V.1

Activities in the field and at the NORSAR Maintenance Center
(1 October 1983 - 31 March 1984)

SA/ Area	Task	Date
03C	Power outage called for subarray visit	22 Nov
02C	LP seismometer and SLEM adjusted	23 Nov
02B (Telem.)	New batteries installed on st. 1, as battery was stolen	24 Nov
01A	Wind measuring equipment disconnected and SP03 and 05 back to normal configuration	25 Nov
NMC	Seismic preamplifiers (6 e.a.) for the PDR-w recorder were built	Nov
NORESS/ NMC	Representatives from Sandia (Dale Breding and Gene Jones) met S. Mykkeltveit and P.W. Larsen at the NMC for discussions. Sandia and NORSAR representatives met consultant in Hamar.	1 Dec
NORESS	In order to clarify unsolved questions, a field survey took place. Participants were Sandia representatives and P.W. Larsen (NMC).	6 Dec 5 Dec
01B	SLEM adjusted and replacement of AHS-card in modem. Latter due to failing B/C-loop.	22 Dec
02B (Telem.)	Battery replaced at the receiving station	23 Dec
NORESS	Replacements of power cable carrying power to instruments in pos. A1, B1 and B5. Most of the period spent on meetings and surveys together with consultant. P.W. Larsen and two other NORSAR representatives (S. Mykkeltveit and R. Paulsen) visited Albuquerque, New Mexico, for meetings and discussions in connection with the New Regional Seismic Array (RSAD). P.W. Larsen spent most of the time on NORESS-related work, i.e., field surveys together with potential contractors, meetings in connection with bidding documents, etc.	9-20 Jan

TABLE V.1 (cont.)

SA/ Area	Task	Date
NORESS	Channel gain increased by 12 dB (all channels)	12 Feb
NMC	Discarded NDPC IBM equipment, temporarily stored at the NMC, was moved to the dealer's premises in Oslo.	28 Feb
03C	DC offset in SLEM all SP channels adjusted. SP channel gain 03, 06 adjusted. Broken data coil NS LP seismometer located.	30 Mar
NORESS	Field supervision, meetings with contractors and consultant	in March
	Construction of foundation for fiber glass tanks started.	-"-
	Drilling of two 60-meter boreholes completed.	

TABLE V.1 (cont.)

Subarray (Normally)	Instr. no. within SA	Ch. no. on NORSAR data tape		Status/time of changes
01A	1	1		8 Hz filter (10/28/82)
(1)	2	2	1) (10/08/82)	
	3	3	2) (11/23/83)	
	4	4		30 dB attenuation
	5	5	3) (11/25/83)	
	6	6		
01B	1	7		
(2)	2	8		
	3	9		
	4	10		
	5	11		
	6	12		
02B	1	13		
(3)	2	14		
	3	15		
	4	16		
	5	17		
	6	18		
02C	1	19		
(4)	2	20		
	3	21		
	4	22		
	5	23		
	6	24		
03C	1	25		
(5)	2	26		
	3	27		
	4	28		
	5	29		
	6	30		

1) Data from borehole at site 1 (60 m borehole) to SP ch 02 (in CTV)
2) Wind meas. equipment disconnected; channel back to original status
3) -"- -"- -"- -"-

TABLE V.2

Status of SP instruments
(1 October 1983 - 31 March 1984)

Subarray (Normally)	Instr. no. within SA	Ch. no. on NORSAR data tape	Status/time of changes
04C	1	31	
(6)	2	32	
	3	33	
	4	34	
	5	35	
	6	36	
06C	1	37	4)
	2	38	
	3	39	
	4	40	
	5	41	
	6	42	

4) 06C comm. line used for transfer of NORESS data to NDPC.

TABLE V.2 (cont.)

VI. DOCUMENTATION DEVELOPED

Iversen, E.: 3-D velocity by use of kinematic and dynamic ray tracing, NORSAR Tech. Rep. 1/84, NTNF/NORSAR, Kjeller, Norway.

Mykkeltveit, S. and H. Bungum: Processing of regional seismic events using data from small aperture arrays, submitted for publication.

Tronrud, L.B.: Semiannual Tech. Summary, 1 Apr - 30 Sep 83, NORSAR Sci. Rep., NTNF/NORSAR, Kjeller, Norway.

L.B. Tronrud

VII. SUMMARY OF TECHNICAL REPORTS/PAPERS PREPARED

VII.1 Study of magnitudes, seismicity and earthquake detectability using a global network

The problem of bias in magnitudes estimated by a network of stations has been addressed in a number of investigations, e.g., Husebye et al (1974), Ringdal (1976), Evernden and Kohler (1976), Chinnery (1978), Christoffersson (1980), Elvers (1980) and Clark (1983). Most of these studies have concluded that the bias problem is indeed significant, especially at low magnitudes. The maximum-likelihood estimation technique described by Ringdal (1976) and Christoffersson (1980) has been shown to reduce the bias significantly. In this paper this method is adapted to a global network of the type reporting to the International Seismological Centre (ISC), and is applied to ten years of ISC data (1971-1980). The revised magnitudes thus obtained are compared to those obtained through conventional estimation techniques, and are also used to develop seismicity recurrence relations and to estimate network detection capability (Ringdal et al, 1977).

The basic model used in this paper has previously been described in detail by Ringdal (1976) and Christoffersson (1980). For further details, we refer to Ringdal (1984).

The data base for this study consisted of the ISC reportings for the 10-year period 1971-1980. At any given time in this period, a typical number of about 1000 seismic stations reported observations to the ISC. An investigation of the station reports confirmed the conclusions of North (1977), who analyzed similar data for the period 1964-1973. Thus, the large majority of stations contribute very few observations, in particular of log(A/T), and would thus be of little use in this study.

For the purpose of magnitude estimation, we found it desirable to select a sub-network of about 100 globally distributed stations. The following basic criteria were applied:

a) Consistent reporting, preferably over the entire 10-year period
b) High detectability, i.e., a large number of teleseismic reports

c) A sufficient number of log(A/T) reports to estimate station parameters
d) Adequate geographical distribution.

Clearly, these criteria were sometimes in conflict. For example, several very sensitive stations, e.g., the large LASA array and some VELA arrays, were only operational for part of the time period, but they were nevertheless selected. Also, the requirements were made less strict for stations in the southern hemisphere, in order to improve geographical coverage. Still, only a few useful stations could be found in Africa and South America. In the end, a total of 115 stations were selected. At any time during the 10 years, about 100 of these were in actual operation.

We note that some stations reported log(A/T) for a low proportion of their detections. It is clearly possible that their detection threshold thus is significantly lower than their threshold for reporting log(A/T). This possibility was investigated for each station by comparing the average ISC event m_b for the total set of reported detections with the average m_b for the subset for which log(A/T) was reported. As a first order approximation, we then adjusted the estimated thresholds according to the difference between these m_b values.

It should be observed that for some of the most sensitive stations, in particular some arrays, many of their reported detections are not associated with detected events in the ISC bulletin. Thus, the thresholds will be too high in these cases. In practice, this will make little difference in the maximum-likelihood procedure since non-detections by these stations for ISC-reported events are usually due to the stations being inoperative. For array stations, we also note that reportings by subarrays or associated stations in some cases replaced the full array reporting.

The previously described method and station network were applied to obtain maximum-likelihood m_b estimates for ISC-reported events during 1971-1980. Known and presumed explosions were removed from the data set so as

not to bias the seismicity estimates. Furthermore, we restricted the data base to only those events which were reported by at least 4 stations of the 115 station network, and which had at least one detection in the distance range 21-100 degrees.

Since out network included most of the better stations reporting to the ISC, the resulting total of about 70 000 events comprised nearly all those events for which any teleseismic reports were included in the ISC bulletins. However, it should be noted that these bulletins also include a large number of events reported by local stations only.

Fig. VII.1.1 shows the resulting frequency-magnitude statistics for shallow events (depth < 60 km) globally. For comparison, similar statistics are also plotted using the magnitude estimation procedure currently employed by the ISC (i.e., averaging observed station magnitudes for all events with at least one log(A/T) report). The large difference in b-values (b=0.90 *vs* b=1.40) illustrates the statistical bias resulting from using conventional magnitude estimation.

Fig. VII.1.1 is quite similar to those obtained when comparing ISC magnitudes to magnitudes reported by sensitive array stations (Chinnery, 1978; Ringdal and Husebye, 1982). Average b-values obtained from array data for large epicentral regions are typically in the range 0.8-1.0, as demonstrated, e.g., for LASA, b ~ 0.84 (Dean, 1972), for NORSAR, b ~ .83 (Bungum and Husebye, 1974) and for the VELA arrays, b ~ 0.93 (Chinnery, 1978). Thus, the results using maximum-likelihood estimation are in good agreement with array studies. However, it must be realized that b-values can show significant regional variations (Evernden, 1970), and considerable caution in interpreting these data is therefore required.

Figs. VII.1.2 and VII.1.3 show incremental and cumulative statistics, respectively, averaged annually for shallow, intermediate and deep earthquakes. The slopes are approximately parallel, and the best-fitting cumulative relationships can be expressed as follows:

$\log_{10}(N_c) = 7.33 - 0.90\ m_b$ $\quad D \leq 60$ km

$\log_{10}(N_c) = 6.85 - 0.90\ m_b$ $\quad 60$ km $< D \leq 300$ km

$\log_{10}(N_c) = 6.13 - 0.90\ m_b$ $\quad D > 300$ km

Here, N_c denotes the cumulative number of earthquakes, and D denotes depth of focus as given by the ISC. Thus, about 70 per cent of global earthquakes are shallow, 25 per cent of intermediate depth and 5 per cent deep. The estimated average annual number of earthquakes globally is about 7500 above $m_b = 4.0$, and the number ranges between 6000 and 9000 for individual years within the ten-year period.

The distribution of estimated m_b bias values compared to conventional m_b estimation is illustrated in Figs. VII.1.4 and VII.1.5. In most cases, conventional m_b values are biased high by between 0 and 0.5 units. Fig. VII.1.5 shows that the bias problem is most significant at intermediate magnitudes. As expected, the bias values decrease somewhat when three or more station reports are required for m_b determination, but are even then significant.

At high magnitudes, our approach gives essentially the same m_b values as those of the ISC. Thus, we have not taken into account the possibility of bias introduced by clipping of strong signals at some stations for such events (Chinnery, 1978; von Seggern and Rivers, 1978). While this problem is important in many contexts, it would not significantly influence the seismicity statistics and detectability estimates in this study.

Based on the estimated magnitude data, an attempt was made to estimate the global teleseismic detectability of shallow events for the 115 station network. For this purpose a regional subdivision of the earth in grids of 15x15 degrees was made, and recurrence statistics for observed shallow earthquakes were considered within each grid area. The method of Kelly and Lacoss (1969) was then used to obtain detectability estimates for regions with sufficient number of observations, and approximate contours were drawn corresponding to these estimates.

Fig. VII.1.6 shows the results for 90 per cent incremental probability of detection at at least four stations. It is seen that the thresholds vary from better than $m_b = 4.2$ over much of the northern hemisphere to $m_b = 4.6$ or higher in parts of the southern hemisphere.

For comparison, the 'Networth' approach (Wirth, 1970) was also applied to the network. The results are shown in Fig. VII.1.7, and can be seen to be in good agreement with those of Fig. VII.1.6.

In some earlier studies, e.g., the report CCD/558, theoretical detection capabilities of global networks were found to be inconsistent with actually reported magnitude data. It would appear that this inconsistency has been largely due to the network magnitude bias problem inherent in conventional magnitude estimation techniques.

The thresholds estimated in this paper relate to <u>average</u> operating conditions of the global network. Under special circumstances, the actual thresholds might be different, e.g., the thresholds would be higher immediately after a large earthquake and during a major aftershock sequence. For this reason, the estimated seismicity levels must also be interpreted with some caution.

As expressed by Ringdal (1976), the maximum-likelihood procedure ideally requires actual measurements of threshold levels at all nondetecting stations for any given event. The statistical approach to thresholds and station downtimes used here has been chosen for practical reasons. However, it has been found by Ringdal (1976) and Christoffersson (1980) that even under very unfavorable circumstances, i.e., during a large aftershock sequence, the maximum-likelihood procedure, using estimated thresholds, produces acceptable results. Thus, while some individual events could be affected by occasional errors in the thresholds, the effect on the total earthquake statistics should be insignificant.

F. Ringdal

References

Bungum, H. and E.S. Husebye (1974): Bull. Seism. Soc. Am., 64, 637-656.

CCD/558 (1978): Report to the Confference of the Committee on Disarmament, Geneva.

Chinnery, M.A. (1978): Tectonophys., 49, 139-144.

Chinnery, M.A. and R.T. Lacoss (1976): In Lincoln Lab. SATS (30 June 1976).

Christoffersson, A.C. (1980): Phys. Earth Planet. Inter., 21, 237-260.

Clark, R.A. (1983): Geophys. J., 75, 545-553.

Dean, W.C. (1972): Tech. Rep. No. 5, Teledyne Geotech, Alexandria, Virginia.

Elvers, E. (1980): FOA Report C 20368-T1, Stockholm, Sweden.

Evernden, J.F. (1970): Bull. Seism. Soc. Am., 60, 393-446.

Evernden, J.F. and W.M. Kohler (1976): Bull. Seism. Soc. Am., 66, 1887-1904.

Husebye, E.S., A Dahle and K.-A. Berteussen (1974): J. Geophys. Res., 79, 2967-2978.

Kelly, E.J. and R.T. Lacoss (1969): Lincoln Lab. Tech. Note 1969-41.

North, R.G. (1977): Lincoln Lab Tech. Note 1977-24.

Ringdal, F. (1976): Bull. Seism. Soc. Am., 66, 789-802.

Ringdal, F. (1984): Paper in preparation.

Ringdal, F. and E.S. Husebye (1982): Bull. Seism. Soc. Am., 72, S201-S224.

Ringdal, F., E.S. Husebye and J. Fyen (1977): Phys. Earth Planet. Inter., 15, P24-P32.

von Seggern, D. and D.W. Rivers (1978): Bull. Seism. Soc. Am., 68, 1543-1546.

Wirth, M.H. (1970): Research Memorandum, Teledyne Geotech, Alexandria, Virginia.

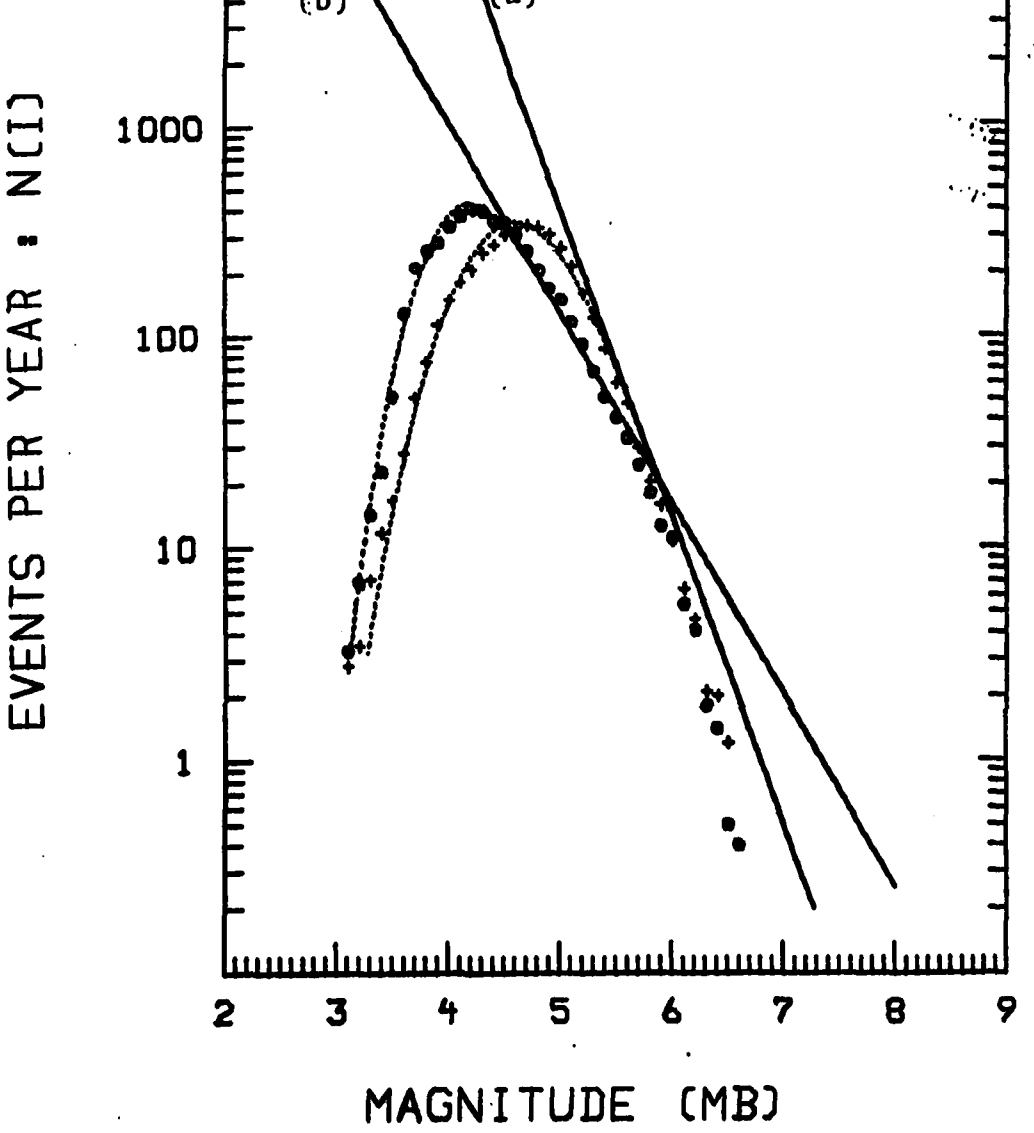

Fig. VII.1.1 Incremental recurrence statistics for shallow events (averaged per year), (a) using conventional m_b (one or more station observations) and (b) using maximum-likelihood m_b. The dotted lines indicate the fit of the Kelly-Lacoss (1969) model. Note the significant difference in slopes between the two cases.

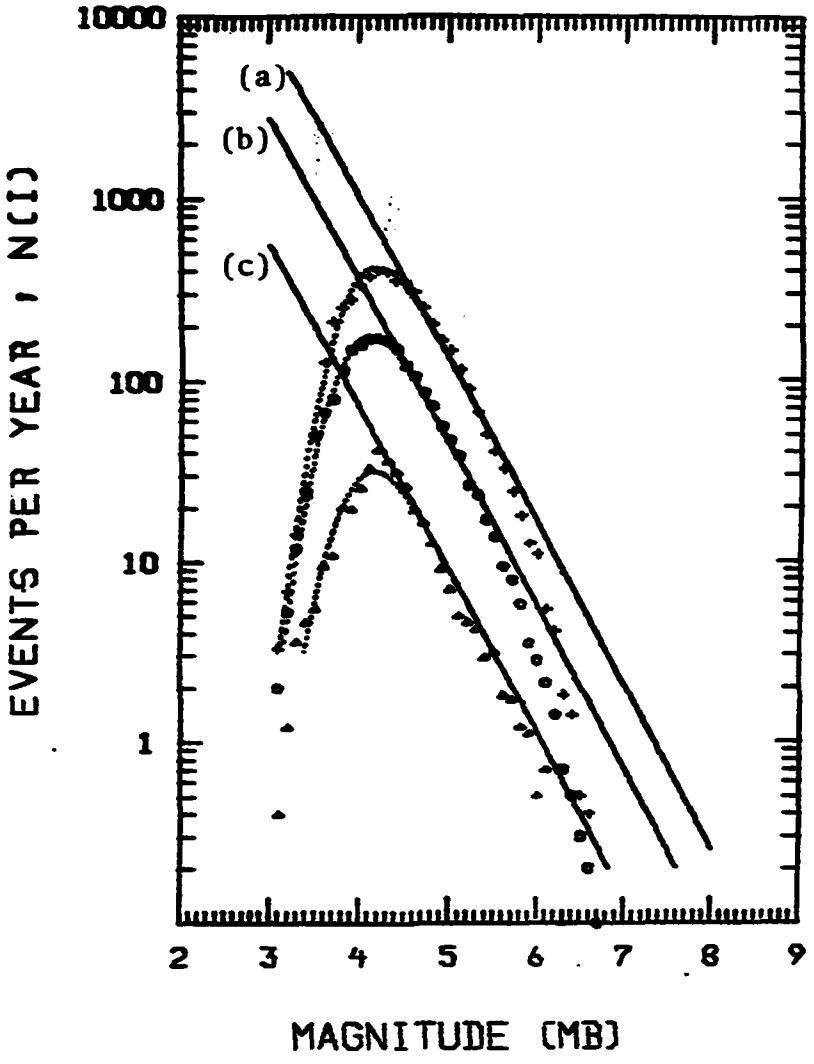

Fig. VII.1.2 Incremental recurrence statistics averaged annually for (a) shallow, (b) intermediate and (c) deep earthquakes globally, using maximum-likelihood mb estimates

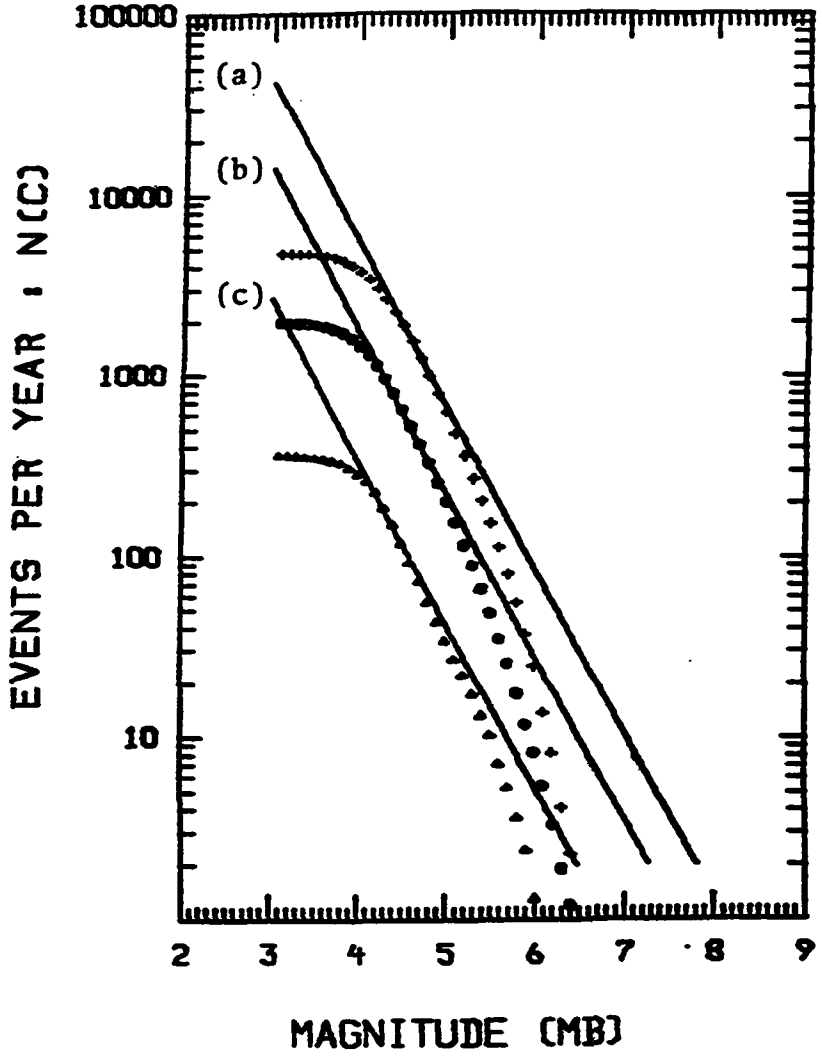

Fig. VII.1.3 Cumulative recurrence statistics averaged annually for (a) shallow, (b) intermediate and (c) deep earthquakes globally, using maximum-likelihood mb estimates.

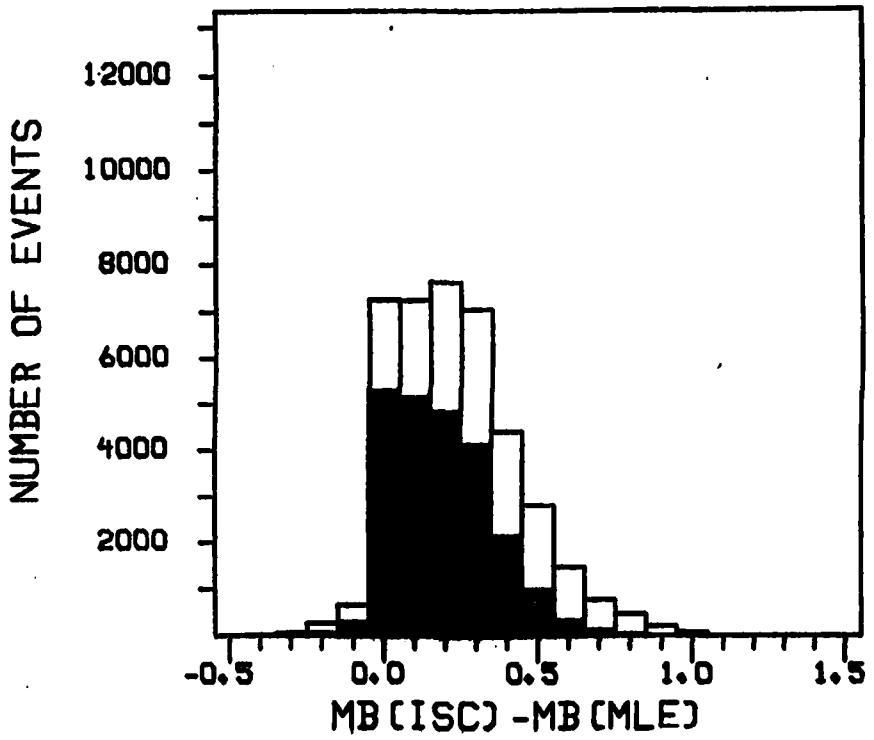

Fig. VII.1.4 Distribution of differences between conventional m_b and maximum-likelihood m_b. The filled columns correspond to requiring at least three observations in the conventional estimates.

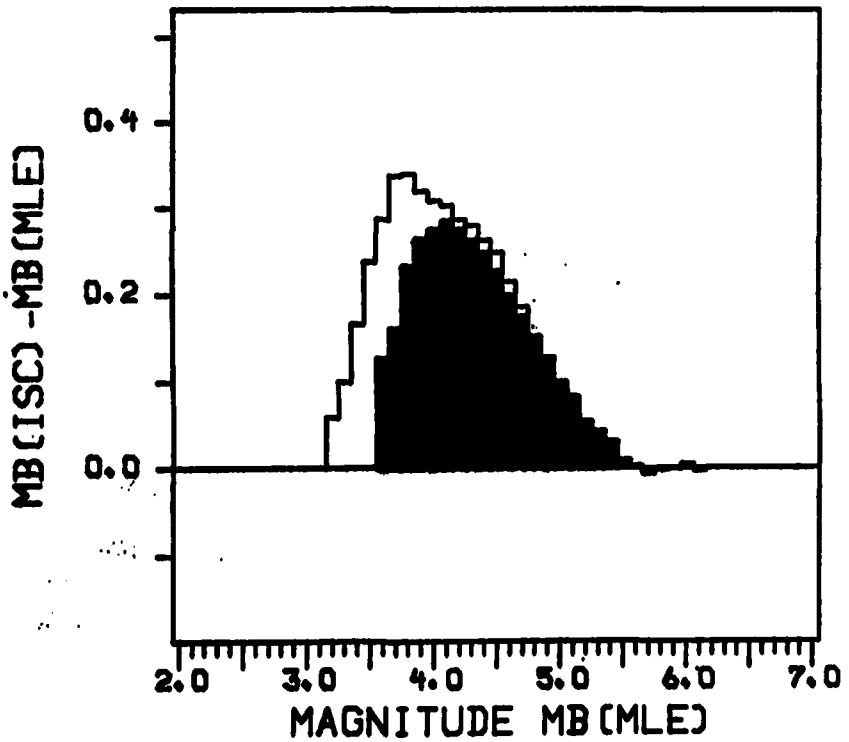

Fig. VII.1.5 Average m_b differences (as in Fig. VII.1.4) shown as a function of maximum-likelihood m_b. Note that the bias is most pronounced at intermediate magnitudes.

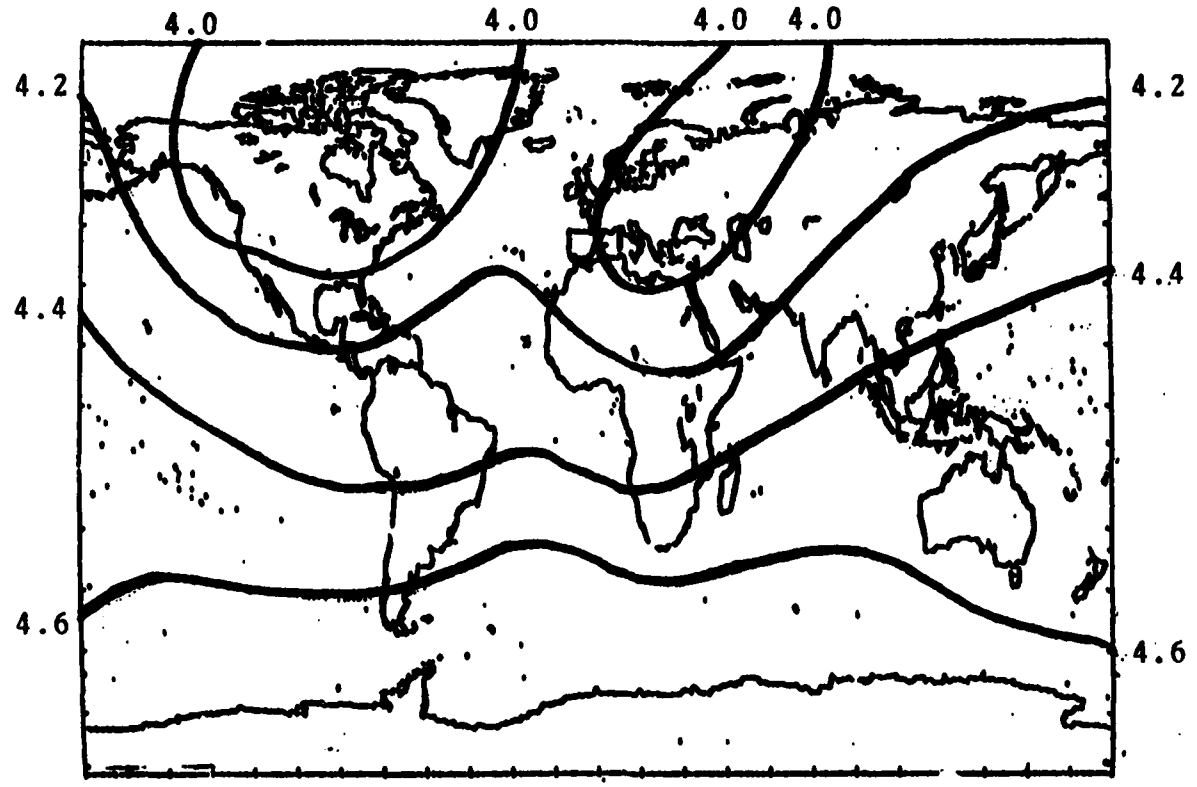

Fig. VII.1.6 Contours corresponding to 90 per cent incremental probability of detection at at least 4 stations of the network, requiring at least 1 teleseismic detection. This figure is based on observed recurrence statistics using maximum-likelihood m_b.

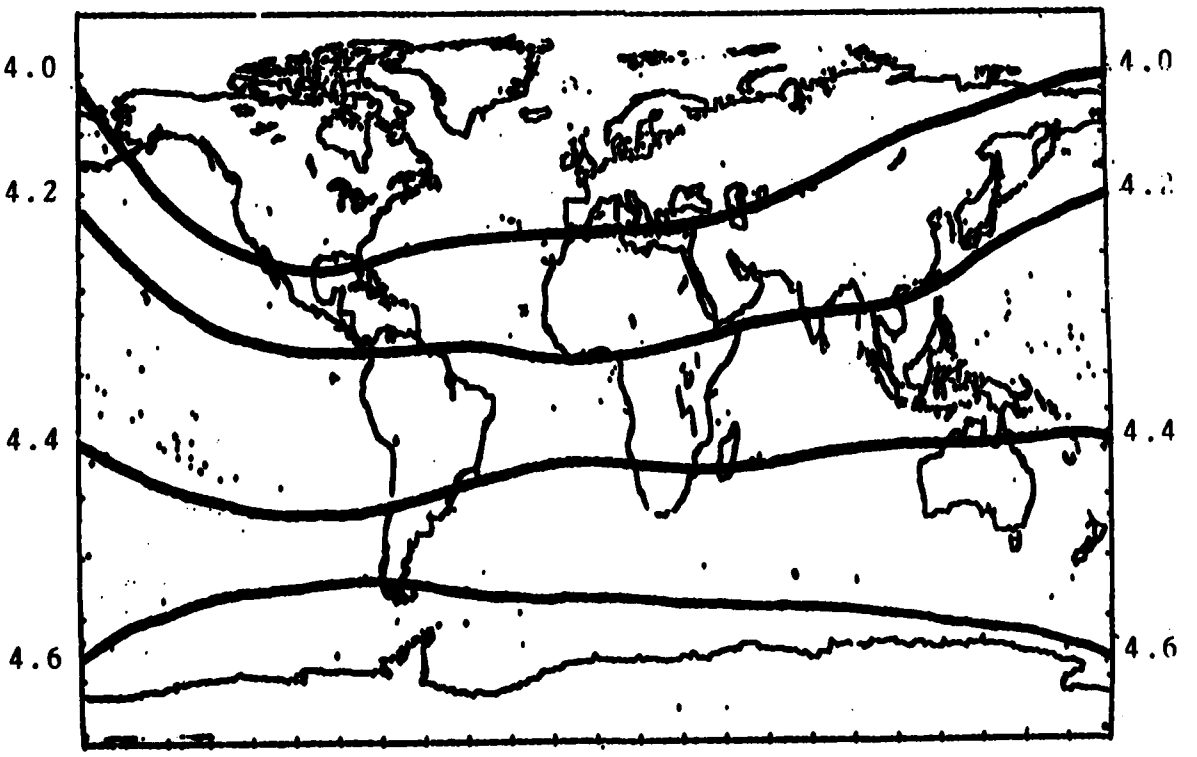

Fig. VII.1.7 Contours corresponding to 90 per cent incremental probability of detection at at least 4 stations of the network, using the 'Networth' approach.

VII.2 Observation and modelling of regional phases recorded at NORSAR

A comprehensive study of propagation characteristics of regional seismic phases for paths to NORSAR is in progress. Such propagation paths intersect with a variety of tectonic provinces like shields and platforms with and without sedimentary covers, orogenic belts, ocean-to-continent transitions, major sedimentary basins and pronounced lateral Moho depth variations associated with graben structures. The study is accompanied by attempts at theoretical modelling of the observed features. The development of the new NORESS array with on-line location of recorded regional events necessitates proper understanding of the general occurrence of secondary phases in particular.

In this contribution, results from an observational and theoretical study on Lg waves across a graben structure in the North Sea are presented. Also included is a short report on the status of comprehensive mapping of regional phases recorded at NORSAR.

Lg waves across the Central Graben of the North Sea

Between 1977 and 1981 a number of large explosive charges were fired in the Central North Sea region in a sequence of seismic refraction experiments carried out by Cambridge University with the object of determining the deep structure of this extensional basin (Fig. VII.2.1). The locations of the shots are indicated on the map of the Central North Sea in Fig. VII.2.1 (top) which also indicates the main structural features and the region where sediment thickness exceeds 2 km. Wood and Barton (1983) have presented a structural model for the Graben region based on the P wave observation from these seismic experiments and detailed information on sedimentary deposits. In this model there is substantial crustal thinning beneath the deepest sediments (Fig. VII.2.1, bottom) with the Moho rising to nearly 20 km depth from 30 km at the flanks to create a crustal pinch. The thinning is accompanied by substantial horizontal gradients in the P wave velocities.

The shots were all clearly recorded at the NORSAR array. For the N shots on the Norwegian side of the Central Graben we get prominent Lg wave arrivals

with a group velocity close to 3.5 km/s for ranges from 430 to 650 km. However, the shots to the west of the graben on the British side (D1, D2, F4), which show very clear P phases, have no distinct Lg arrivals.

The vertical component records for each of these explosions at the 02C03 seismometer at NORSAR are displayed in Fig. VII.2.2, after bandpass filtering with 3 dB points at 1.5 and 5 Hz. The traces are all normalized to the same maximum amplitude, the range is indicated to the right, and the time corresponding to a group velocity of 3.5 km/s is indicated by an arrow on each trace. The abrupt change in the character of the records as the shot points cross the Central Graben is very pronounced. For shots D1, D2 and F4 there is a slight increase in amplitude in the coda for group velocities around 4.2 km/s which is somewhat slower than a direct Sn path. For sources in Germany at similar ranges clear Lg waves are seen so that we do not have an explanation by range alone.

In order to try to understand the extinction of the Lg wave in crossing the graben zone, a number of numerical experiments have been conducted using the calculation scheme introduced by Kennett (1984). The S-wave train is represented as a superposition of higher mode surface waves for a reference structure and the way in which energy is transferred between modes as the wave train interacts with a heterogeneous zone is followed. The changes in relative modal amplitude modify the transmitted waves and there is also coupling to backward travelling modes giving rise to reflected waves. In view of the uncertainties in the shear wave speeds in the zone of crustal thinning, we have not attempted to use the Wood and Barton model directly. We have developed a simplified model shown in Fig. VII.2.3 with a sedimentary zone thickening from 2 km to 9 km with the same properties as the surface sediments. In the lower part of the crust we introduce material with properties close to those in the mantle (ρ = 3.2 Mg/m^3, β = 4.3 km/s) reducing the crustal thickness to 21 km. The reference stratified model outside the graben zone was the modified form of a model due to Bouchon (1982) discussed in Kennett (1984). In order to allow us to represent all shear waves with group velocities slower than 5.0 km/s

by means of a modal representation, we have extended the model to 70 km depth and then introduced a half-space with shear wave speed 5.0 km/s.

The main trend of the structural features in the central North Sea is close to perpendicular to the paths to NORSAR. We are therefore able to use a two-dimensional model as a very good approximation to the actual situation. In order to simplify the already complicated calculations we have considered SH wave propagation through the model. As discussed in Kennett (1984) the close parallel between the behavior of the vertical component in Rayleigh mode propagation and the transverse component in Love mode propagation means that our results can be compared directly to the observations.

We have considered three different models for the effect of the graben structure. In the first (A) we have included only the thickening sediments and maintained the Moho depth at 30 km throughout, with no heterogeneity in the lower crust. The second model (B) was as illustrated in Fig. VII.2.3, with both sediment thickening and substantial crustal thinning. For both cases A and B we work with perfect elasticity. However, in order to give a better representation of the complex structure we also consider a further model (C) in which the structural model B is combined with a loss factor $Q_\beta^{-1} = 0.02$ over the span of the model from 0 to 110 km. The consequent attenuation is quite severe, but is intended to provide a measure of the effect of the complex, faulted structure to be found in the neighborhood of the crustal pinch.

Results of the detailed calculations for the three different models are presented in Kennett and Mykkeltveit (1984). We have illustrated the propagation of a 1 Hz wave train through the model; at this frequency there are 19 modes with group velocity less than 5 km/s. Of these, modes 1-10 represent Lg type propagation and modes 11-18 represent Sn waves with most of their energy in the upper mantle. This frequency provides a reasonable compromise between having a diverse collection of modes, representative of high frequency behavior, and reasonable computation cost. At 1 Hz, the

fundamental mode is confined to the sediments and so we work with 18 x 18 matrices of reflection and transmission coefficients between the different modes. Once these matrices have been calculated we can determine the effect of any incident field by the action of the reflection or transmission matrix on the vector of incident modal amplitudes.

When we compare the results of these calculations with the record section in Fig. VII.2.2 we find (Kennett and Mykkeltveit, 1984) that we have been able to give a reasonable match to the observed behavior. The character of the modal train transmitted through the thinning crust models will be profoundly different from the incident wavefield and the energy in Lg will be much reduced compared with paths which do not cross the feature. By taking a simplified structural model of the central graben zone based on that proposed by Wood and Barton (1983) we find that it is possible to achieve a significant transfer of energy out of Lg type modes into upper mantle propagation. Such energy arrives quicker than before, so that the onset of Lg is obscured by earlier arrivals while the peak amplitude is reduced. The overall effect is to smear out the S wave energy over a wide range of group velocities and by transferring energy from the most energetic components to destroy the normal interference pattern which gives rise to the characteristic Lg arrivals. In addition to the bulk structural effects, attenuation due to wave scattering in the faulted central zone and enhanced anelastic loss due to higher heat flow through the thinner crust will help to diminish the transmitted Lg wave energy.

General mapping of regional phases recorded at NORSAR

In many circumstances where the Lg phase is not observed, crustal barriers to propagation are postulated, but it is often difficult to be precise about their location. With a sequence of shots crossing a structural feature, as in the results presented above, it is possible to identify the cause of the poor transmission of Lg waves with observations at a distant receiver. By using many events and stations it is possible to build up an areal picture of the pattern of crustal heterogeneity from the character of the Lg train. Gregersen (1984) has mapped Lg propagation in the North Sea region

and identified features representing barriers to propagation of this phase. His data base is presently being supplemented with new (particularly NORSAR) data in order to obtain an even more complete picture of propagation characteristics in the North Sea and adjacent regions.

For a general study of propagation to NORSAR from regional distances, records from events up to 15°-20° away are now being compiled, and inspected for assessment of propagation characteristics of regional phases. A proper mapping and understanding of the relative strengths of the Lg and Sn phases is of particular importance to the performance of the on-line processing of regional events on the new NORESS array. Fig. VII.2.4 gives examples of NORSAR records for three events at approximately the same distance (12°) but with differing azimuths, exhibiting marked differences in the occurrence of the secondary phases Sn and Lg. Processing of detected signals on the new NORESS array is based on FK-analysis for the phase identification, and since Sn and Lg cannot be separated on the basis of phase velocities alone, it will be necessary to invoke information on the general occurrence and relative strength of secondary phases for different source regions. Once such information has been compiled, it will be built into the event location part of the on-line processing package for NORESS.

S. Mykkeltveit
B.L.N. Kennett, Univ. of Cambridge, UK

References

Bouchon, M. (1982): The complete synthesis of seismic crustal phases at regional distances, J. Geophys. Res., 87, 1735-1741.

Gregersen, S. (1984): Lg wave propagation and crustal structure differences near Denmark and the North Sea, Geophys. J.R. astr. Soc., 79 (in press).

Kennett, B.L.N. (1984): Guided wave propagation in laterally varying media, I: Theoretical development, Geophys. J.R. astr. Soc., 79 (in press).

Kennett, B.L.N. and S. Mykkeltveit (1984): Guided wave propagation in laterally varying media. II: Lg waves in Northwestern Europe, Geophys. J.R. astr. Soc., 79 (in press).

Wood, R. and P. Barton (1983): Crustal thinning and subsidence in the North Sea. Nature, 302, 134-136.

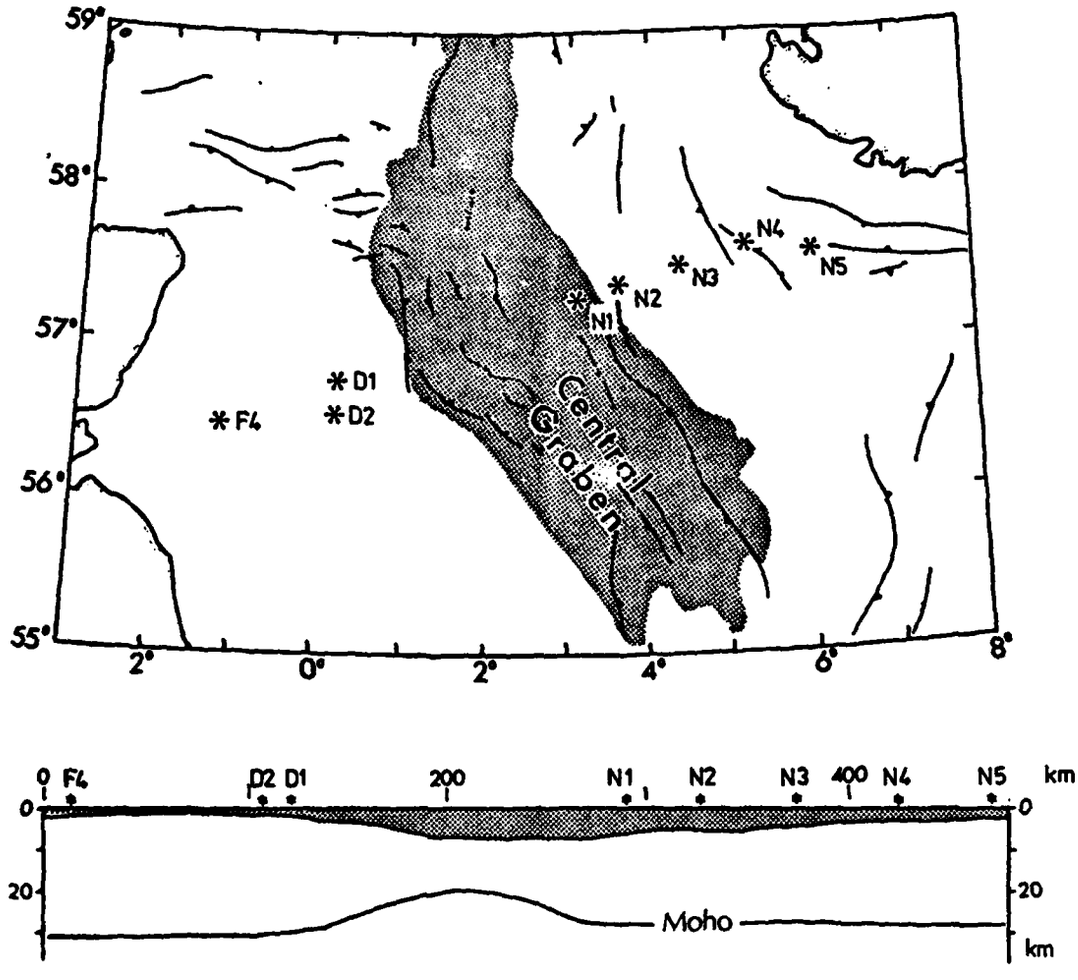

Fig. VII.2.1 Top: Map of the central North Sea basin showing the main structural features. The Central Graben zone with sediments thicker than 2 km is indicated by shading. The positions of the major shots in the seismic refraction experiments are indicated by stars.

Bottom: Cross section of structure across the graben zone along the line of the shots proposed by Wood and Barton (1983).

Sediments are indicated by shading.

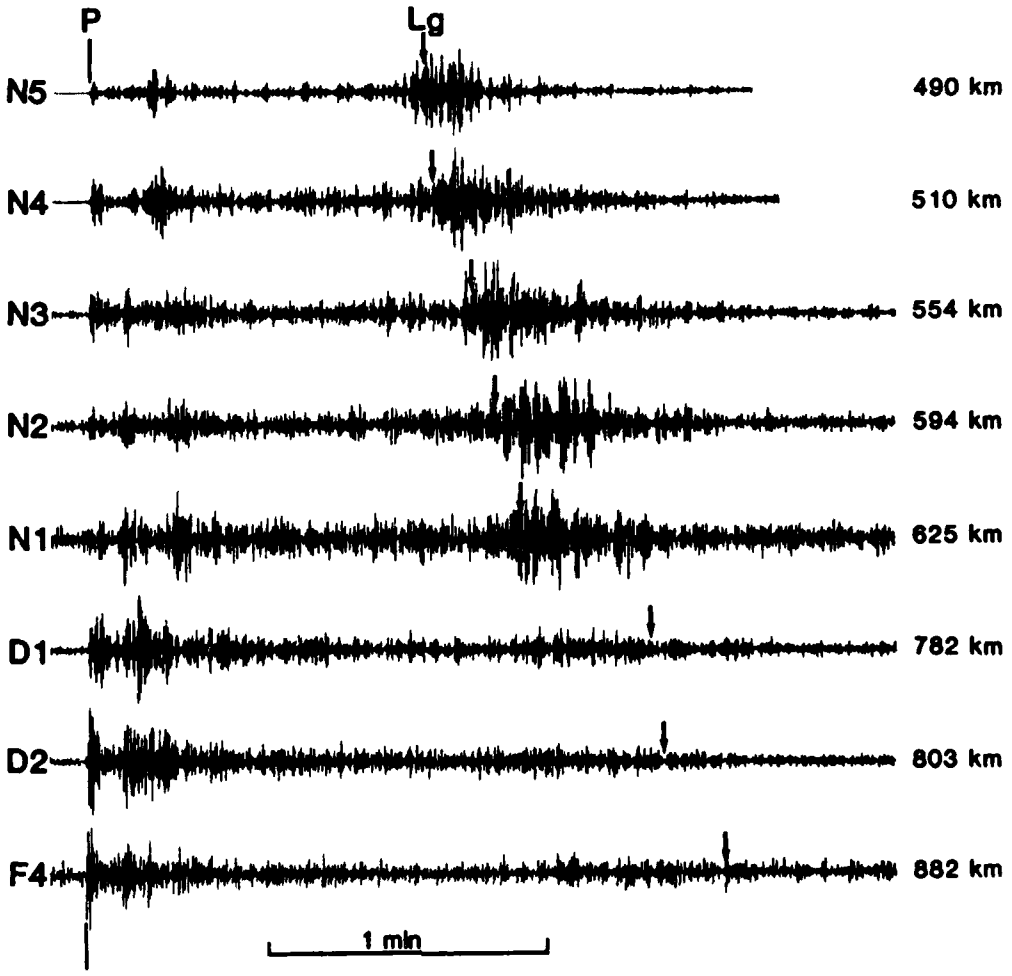

Fig. VII.2.2 Record section of seismograms from the major refraction shots spanning the Central Graben zone marked in Fig. VII.2.1. Each trace is normalized to the same maximum amplitude and aligned on the P wave onsets. An arrow indicates a group velocity of 3.5 km/s corresponding to Lg wave arrivals.

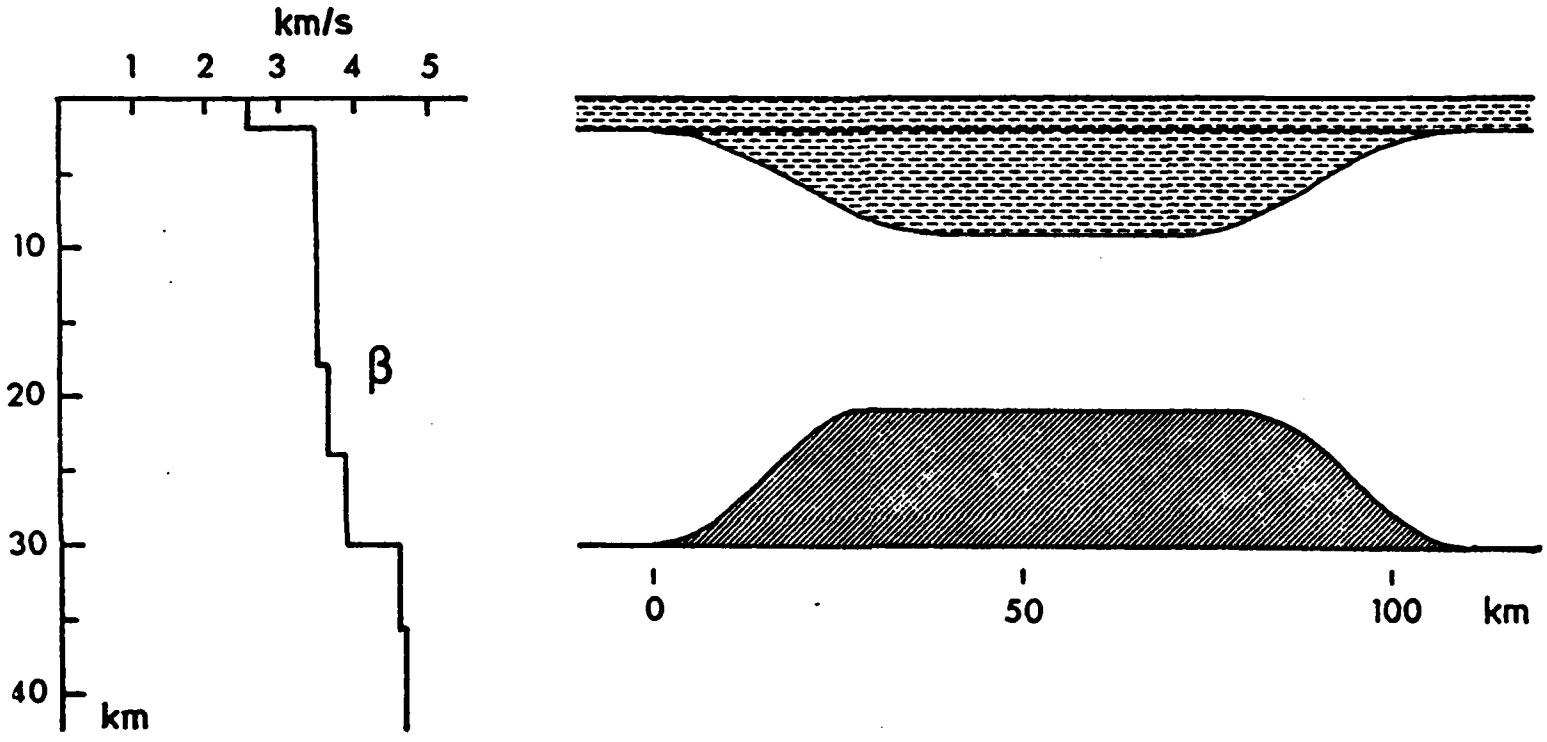

Fig. VII.2.3 Shear velocity model for the reference stratification and illustration of the structural model used in the study of Lg propagation across the graben zone.

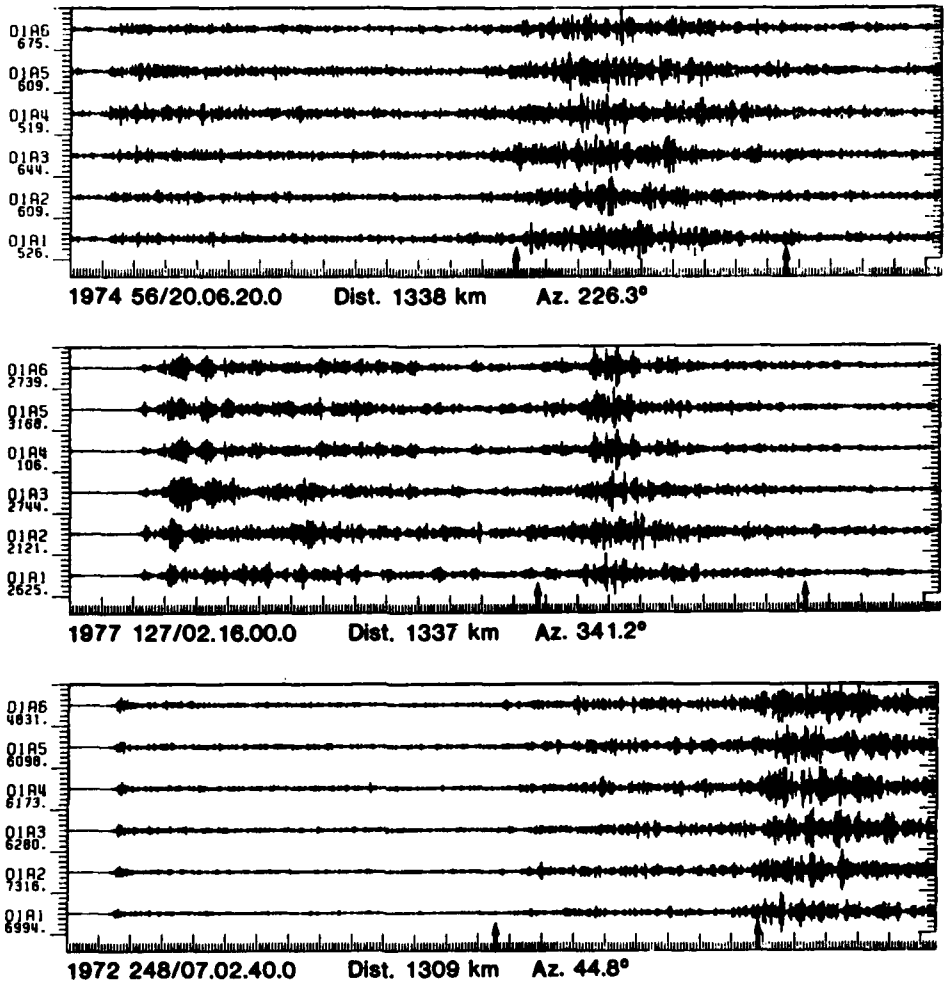

Fig. VII.2.4 Three events recorded at the NORSAR subarray 01A (6 instruments within a diameter of 10 km). All data have been bandpass fitered 1.2-3.2 Hz. For each event the two arrows indicate group velocities of 4.5 km/s and 3.5 km/s. Data start time, epicentral distance and station-to-epicenter azimuth are given for each event. The three events originated in the United Kingdom (top), in the Jan Mayen Island region (middle) and on the Kola peninsula in western Russia. As can be seen from the records, the relative strength of secondary phases Sn (standard group velocity about 4.4-4.5 km/s) and Lg (group velocity 3.5 km/s) varies drastically between various propagation paths to NORSAR. The traces are plot normalized with scaling factors given to the left. At the time of the 1977 event, channel 01A4 recorded data from channel 01A6, attenuated 30 dB. Data window length is 275 seconds in all three frames.

VII.3 On the determination of radiated seismic energy and related source parameters

The determination of radiated seismic energy on the one hand, and of source size and static stress drop on the other, depends in principle on a representation of different parts of the source spectrum. In practice with band-limited data from a sparse network the required source parameterization is often the same. Spectral models parameterized by the source's central moments of degree zero and two are introduced as an approximation to the general representation of the amplitude spectrum in terms of the central moments of even degree. Phase spectra are not used, apart from polarity which is determined by a correlation method. These models are shown to simulate well the principal features of common circular and Haskell type models, including the corner frequency shift of P waves with respect to S waves, and the relation between rupture velocity and maximum seismic efficiency. Spectral bandwidth and the determination of radiated energy and apparent stress are contrasted to time domain pulse widths and the determination of source size and static stress drop in these models. In the last semi-annual report we discussed the determination of spectral bandwidth and pulse width. Radiated energy and apparent stress are determined from a far-field representation involving the spectral bandwidth; source size and static stress drop are determined from a relation between the second central moments λ_x^2, λ_y^2 and an elliptical surface under uniform stress drop, i.e., we find the equivalent surface for uniform stress drop

$$S_\sigma = 5\pi\ \lambda_x\lambda_y \qquad (1)$$

and an estimate of the static stress drop is then

$$\Delta\sigma = 3M/(10\sqrt{5}\ \pi C\lambda_x\lambda_y^2) \qquad (2)$$

where M is the scalar moment and the nondimensional constant C is a function of ellipticity λ_y/λ_x. Determining these parameters with a Gaussian spectral model gives results consistent with the limits imposed by

cohesive cracks, i.e., the maximum seismic efficiency approaches one for rupture velocities near the limiting values (Rayleigh velocity for in-plane strain, S velocity for anti-plane strain). One of the results is shown in Fig. VII.3.1. An ω-square model, although having more acceptable asymptotic properties, does not lead to these physically consistent results.

Since real data often require the number of source parameters to be limited, it is of practical interest to examine the consequences of a reduced number of parameters, in particular for circular models and point source approximations; in these cases results for radiated energy can be obtained in closed form. A comparison is given in Fig. VII.3.2, where the finite source and corresponding point source model have equivalent spectral bandwidth for P or S. Some general conclusions are as follows: "Equivalent" point source models severely underestimate the radiated energy from sources with strong directivity effects (e.g., Haskell type of models with rupture velocity near the limiting values), but they can give a useful approximation (within a factor of two) to the radiated energy from sources with relatively weak directivity effects (e.g., the class of circular models). It is possible to correct for the "point source bias" assuming a fixed directivity coefficient d (which is a function of source shape and rupture velocity). However, if d is fixed it follows that the seismic efficiency is also fixed, i.e., apparent stress will then be a fixed fraction of the static stress drop.

If the stress drop is constant and earthquake sources are geometrically and dynamically similar, then seismic energy scales linearly with moment. There is observational evidence both for and against the simple scaling relations. Source complexity will in general change these relations, unless the statistical irregularity of faulting follows a particular form of self-affinity. In a stochastic model characterized by some typical correlation distance of faulting, the scaling may be between linear and quadratic, and so the apparent stress would be

between constant and linearly increasing with moment. Fig. VII.3.3 shows the results for a particular stochastic model specified in a recent paper (Doornbos, 1984). The results imply that a relatively large increase of radiated energy with moment would be accompanied by an underestimate of source size and an overestimate of stress drop. This bias is related to the misinterpretation of corner frequencies of complex faults, as noted by several authors (e.g., Madariaga, 1979). However, the determination of radiated energy may still be correct.

D.J. Doornbos

References

Doornbos, D.J. (1984): On the determination of radiated seismic energy and related source parameters. Bull. Seismol. Soc. Am., in press.

Madariaga, R. (1979): On the relation between seismic moment and stress drop in the presence of stress and strength heterogeneity. J. Geophys. Res., 84, 2243-2250.

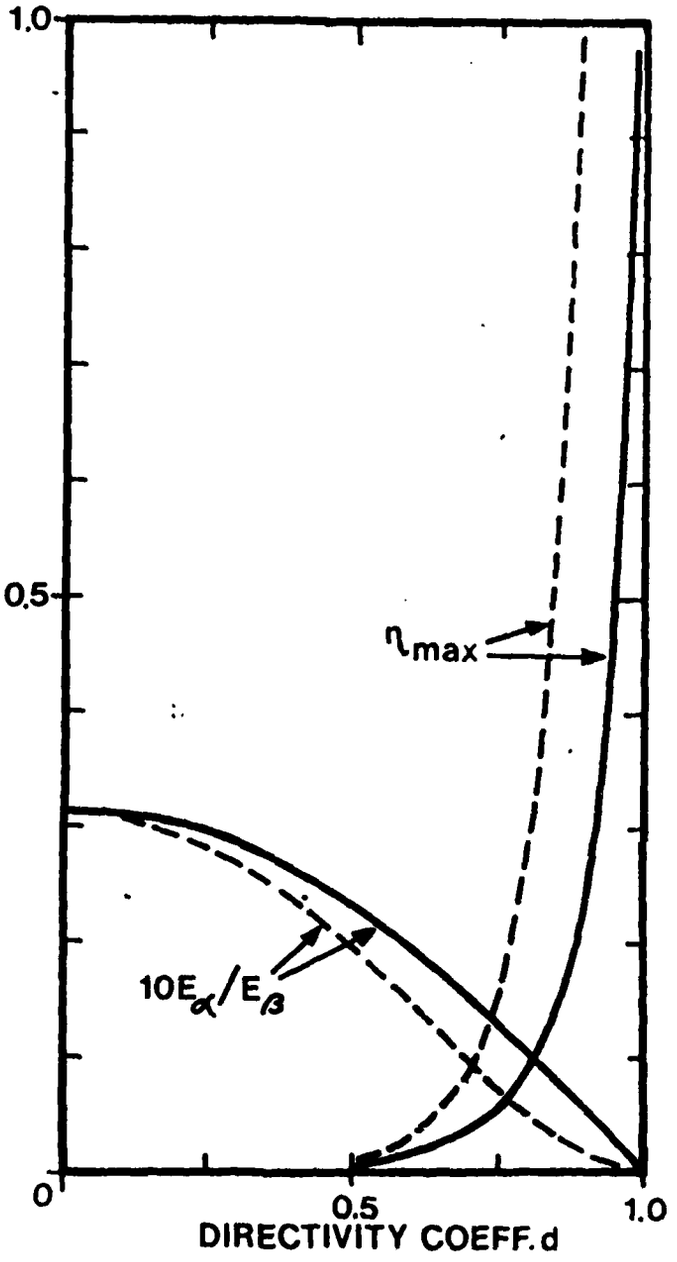

Fig. VII.3.1 Maximum seismic efficiency η_{max}, and ratio of P to S radiated energy E_α/E_β (multiplied with factor 10), versus directivity coefficient d. If d = 1, rupture velocity equals S velocity. Moment tensor approximation to Haskell unidirectional model, in combination with a Gaussian spectral model. The aspect ratio is 0.4.
_____ : transversal slip; _ _ _ _ _ : longitudinal slip.

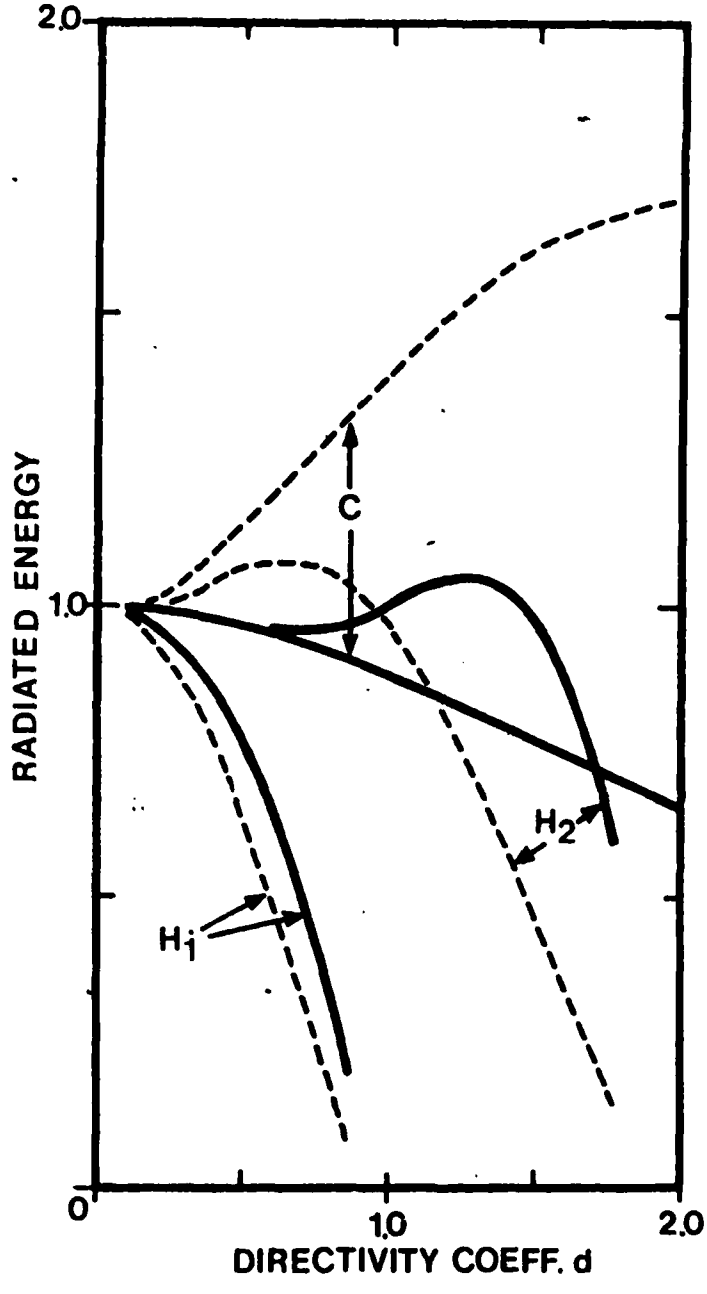

Fig. VII.3.2 Radiated seismic energy for point source approximations to Haskell unidirectional model (H1), Haskell bidirectional model (H2), circular model (C). Aspect ratio of Haskell models is 0.4. If rupture velocity equals S velocity, d = 1 in model H1, d = 2 in model H2 and d ≈ 1.5 in model C. Point source approximations are equivalent with respect to spectral bandwidth for S (_____) or P (_ _ _ _). The curves give the fraction of radiated energy in relation to that of the true model.

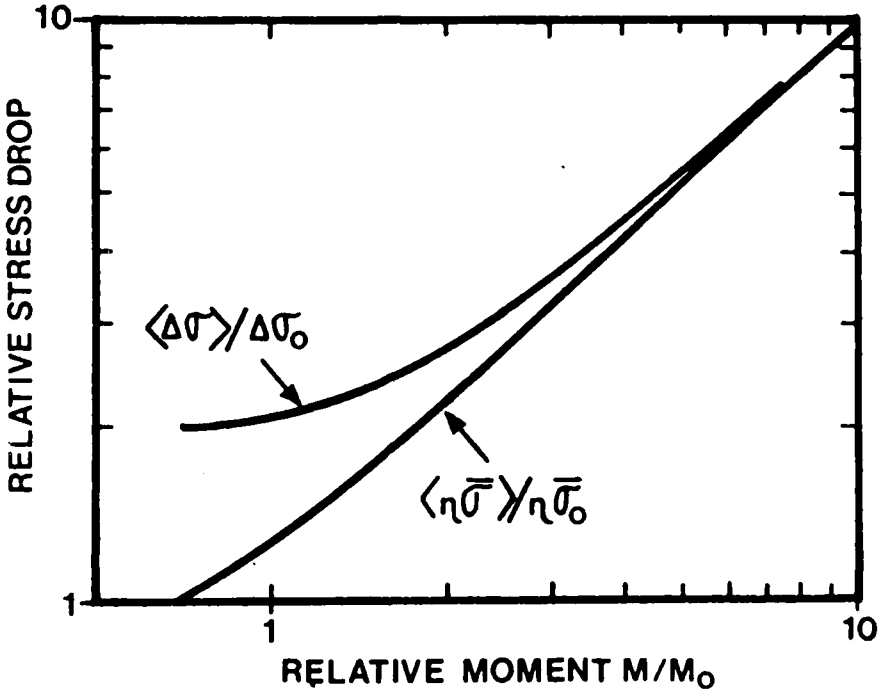

Fig. VII.3.3 Apparent stress and stress drop versus moment of complex faults. The source is characterized by a stochastic part determining the spatial and temporal scale of faulting, and a deterministic part determining the spatial extent of the whole source; for details see Doornbos (1984). The reference moment and stress drop (M_o, $\eta\sigma_o$, $\Delta\sigma_o$) are for a coherent subfault with scale lengths corresponding to those in the stochastic model.

VII.4 Fennoscandian seismicity, 1980-84

As a part of our efforts to develop a frame of reference for the NORESS data, included what is needed in order to assess the capabilities of that array, an extensive study is now being conducted with the purpose of investigating the natural seismicity at regional distances from the array, as well as to monitor the largest explosions in the area. The effort involves close cooperation between NORSAR and the University of Bergen and the British Geological Survey (Edinburgh), all of which are contributing with data and readings from their respective seismic stations. It is our intention to continue this cooperation in the years to come by continuously updating the data file.

The data base contains presently around 10500 individual station readings from about 430 events. About 340 of these have been classified as earthquakes, and 45 have been felt by people. The data base is complete for events above local magnitude (M_L) 2.5, while events below this level have been included only if we are reasonably sure that they are not man-made. In Fig. VII.4.1 we have shown the earthquake locations from this data base (M_L>2.0), indicating a strong concentration of events along, and west of, the west coast of Norway. In comparing with previous seismicity studies, it should be noted that the present one has significantly better detection thresholds and precisions in event locations. It is also noteworthy that by the inclusion of stations on both sides of the North Sea (including the Shetland Islands) we have more or less removed the significant east-west bias that previous catalogues have contained, and the result (cf. Fig. VII.4.1) is an even stronger tendency towards offshore locations.

The frequency-magnitude distribution for the earthquakes plotted in Fig. VII.4.1 is shown in Fig. VII.4.2. The figure shows a b-value of around -0.9 (note: M_L magnitudes), and it can be seen from the figure that the catalogue is fairly complete down to a magnitude of about 2.3. Events with M_L>2.5 are finally listed in Table VII.4.1.

H. Bungum
B.K. Eikland

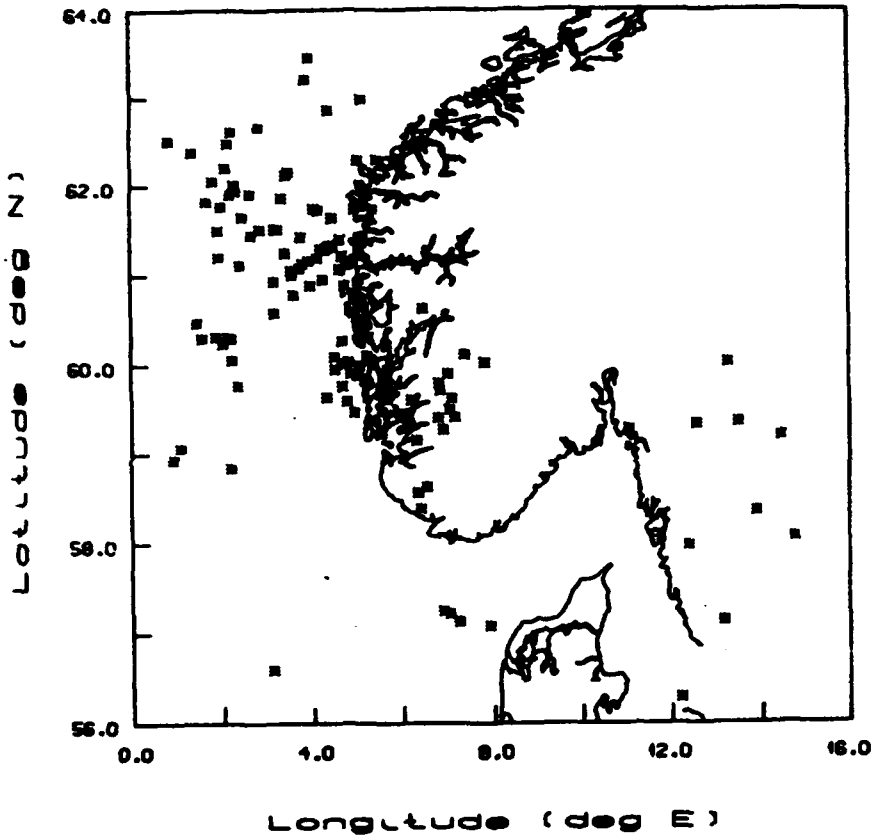

Fig. VII.4.1 Earthquake locations for earthquakes (M_L>2.0) reported from 1980 to 1984 using seismic stations in Scandinavia and in Great Britain.

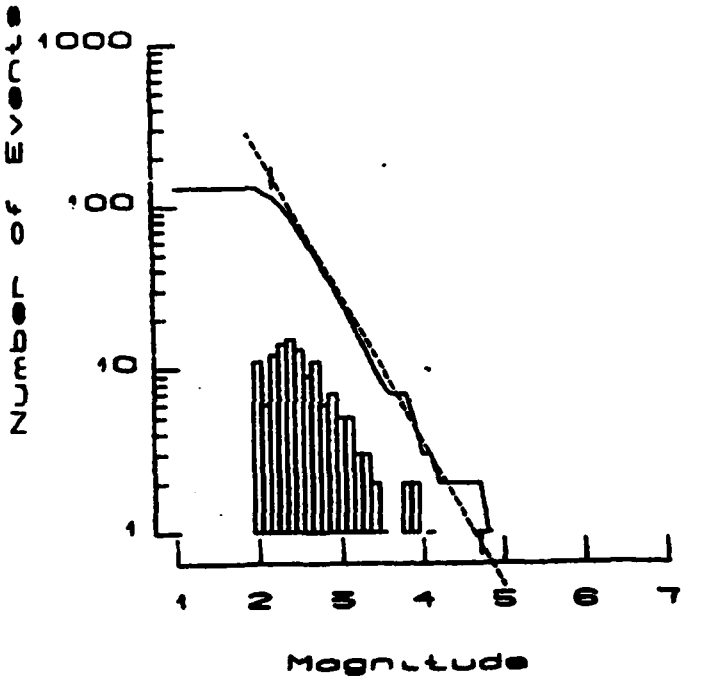

Fig. VII.4.2 Frequency-magnitude distribution for the earthquakes plotted in Fig. VII.4.1.

YEAR	DATE	AGENCY	OR.TIME	LATIT.	LONGIT.	ML-	REF	FELT	NST
1980	JAN 21	NAO	74135.7	56.276N	12.220E	2.7	NAO		14
1980	MAR 14	NAO	456 6.6	61.286N	4.320E	3.0	NAO	F	21
1980	MAR 30	NAO	35345.5	62.670N	2.817E	2.5	BGS		9
1980	APR 11	NAO	41912.4	57.974N	12.391E	2.6	NAO	F	15
1980	MAY 2	NAO	22 548.8	62.984N	5.091E	3.0	NAO		18
1980	MAY 9	NAO	234230.7	61.939N	2.311E	3.5	BGS		14
1980	MAY 27	NAO	204335.9	61.819N	1.665E	2.9	NAO		17
1980	JUN 2	NAO	164419.9	62.115N	3.412E	2.8	UPP		12
1980	JUN 5	NAO	10 8 4.9	61.251N	5.065E	2.9	UPP		5
1980	JUN 8	NAO	758 8.1	60.776N	3.608E	4.1	UPP	F	36
1980	JUN 11	NAO	72227.4	58.935N	0.953E	3.2	BGS		7
1980	JUN 18	NAO	15 625.5	60.944N	4.252E	2.9	NAO		17
1980	JUL 16	NAO	181054.2	59.394N	6.807E	2.7	UPP		5
1980	AUG 1	NAO	85821.2	59.403N	7.182E	2.7	NAO		14
1981	MAR 9	NAO	46642.0	61.722N	5.361E	3.1	BGS	F	14
1981	APR 16	NAO	63819.8	61.107N	2.410E	2.5	NAO		8
1981	APR 29	NAO	3 851.6	61.299N	4.354E	2.5	BGS		5
1981	APR 29	NAO	194045.6	59.624N	4.332E	2.8	NAO		4
1981	JUN 9	NAO	234216.8	61.046N	3.546E	2.7	NAO		4
1981	JUN 9	NAO	2347 5.9	61.419N	3.762E	2.7	NAO		7
1981	JUN 15	NAO	125247.5	60.237N	2.027E	2.9	BGS		7
1981	JUN 28	NAO	71659.8	63.217N	3.847E	2.6	BGS		3
1981	JUN 30	NAO	123210.5	58.348N	13.893E	2.0	NAO		5
1981	JUL 4	NAO	112640.7	61.153N	3.923E	2.8	NAO		7
1981	AUG 13	NAO	23 120.9	61.069N	3.735E	2.5	SNN		3
1981	SEP 6	NAO	412 0.9	57.125N	7.255E	3.9	UPP		11
1981	OCT 8	NAO	153535.7	59.594N	6.221E	2.5	NAO		5
1981	NOV 11	NAO	24851.5	57.129N	13.155E	2.9	UPP	F	10
1981	NOV 30	NAO	11 156.5	61.498N	1.914E	3.1	BGS		4
1982	JAN 4	NAO	1822 6.9	59.217N	5.561E	2.9	NAO	F	14
1982	FEB 6	NAO	45042.5	61.057N	4.619E	2.7	NAO		5
1982	FEB 7	NAO	136 3.3	61.321N	4.400E	2.5	NAO		5
1982	FEB 9	NAO	132326.1	59.890N	4.881E	2.6	NAO		5
1982	MAR 15	NAO	135711.5	60.013N	13.273E	2.5	NAO	F	14
1982	MAR 17	NAO	223314.8	62.202N	2.070E	3.1	NAO		14
1982	APR 7	NAO	18 837.9	59.611N	7.110E	3.1	BGS	F	19
1982	APR 19	NAO	94926.0	61.718N	4.133E	3.9	BGS	F	21
1982	APR 20	NAO	131929.7	59.143N	6.332E	3.8	BGS	F	20
1982	MAY 10	NAO	211641.6	60.090N	5.243E	2.6	NAO		11
1982	MAY 10	NAO	2125 9.6	60.037N	5.303E	2.6	NAO		11
1982	MAY 30	NAO	1 250.7	61.444N	2.675E	2.7	BGS		5
1982	JUN 11	NAO	029 3.3	56.585N	3.106E	2.7	BGS		9
1982	JUL 29	NAO	017 2.5	60.308N	2.131E	4.8	BGS	F	63
1982	AUG 6	NAO	74124.9	60.615N	6.492E	3.4	NAO	F	18
1982	NOV 4	NAO	656 9.1	62.487N	2.127E	2.5	BGS		8
1982	NOV 23	NAO	165837.6	60.576N	3.177E	2.5	NAO		5
1982	DEC 6	NAO	144332.5	60.020N	4.820E	2.5	NAO		14
1982	DEC 15	NAO	64441.7	62.284N	5.454E	3.8	NAO	F	26
1982	DEC 27	NAO	1815 6.1	61.198N	1.935E	3.1	NAO		0
1983	FEB 13	NAO	245 3.5	61.243N	3.413E	2.5	NAO		15
1983	FEB 24	NAO	41947.0	60.314N	1.870E	3.0	NAO		19
1983	MAR 8	NAO	184357.3	59.725N	5.632E	4.7	NAO	F	25
1983	MAR 8	NAO	1852 6.8	59.756N	5.637E	3.0	NAO		14
1983	MAR 31	NAO	44624.0	61.397N	5.139E	2.8	NAO		23
1983	MAY 8	NAO	174738.9	61.282N	4.202E	2.9	NAO		7
1983	MAY 12	NAO	41557.1	59.780N	6.838E	3.3	NAO		16
1983	JUL 12	NAO	19 427.7	58.054N	14.762E	2.5	NAO	F	9
1983	AUG 8	NAO	1557 9.6	61.734N	4.038E	3.2	NAO		9
1983	OCT 1	NAO	75135.2	60.293N	2.204E	2.8	NAO		13
1983	OCT 7	NAO	94042.8	59.264N	6.919E	2.6	NAO		6
1983	OCT 7	NAO	19 357.1	63.471N	3.928E	3.0	NAO		12
1983	OCT 29	NAO	1751 4.9	59.883N	7.038E	3.3	NAO	F	7
1983	DEC 11	NAO	74546.4	62.617N	2.205E	2.7	NAO		12
1983	DEC 16	NAO	21 923.8	62.857N	4.343E	3.4	NAO		19
1984	JAN 1	NAO	211553.5	59.579N	4.788E	2.7	NAO		8
1984	JAN 6	NAO	95119.7	59.453N	4.953E	2.6	NAO		7
1984	JAN 7	NAO	9 811.8	57.209N	7.044E	3.2	NAO		17
1984	JAN 13	NAO	25346.9	61.179N	4.128E	2.8	NAO		4
1984	FEB 5	NAO	11 817.6	60.997N	3.564E	2.7	NAO		8
1984	FEB 14	NAO	104217.6	61.904N	2.635E	3.3	NAO		9
1984	MAR 1	NAO	132455.6	60.003N	4.764E	2.6	NAO		7
1984	MAR 1	NAO	154138.4	60.005N	4.683E	2.6	NAO		8

Table VII.4.1 Earthquakes with M_L>2.5 from the data base plotted in Fig. VII.4.1.

VII.5 Source parameter analysis, 8 March 1983 Stord earthquake

Among the events in the data base presented in VII.4, we have the best recorded Norwegian earthquake to date, from March 8, 1983 (M_L = 4.7). The large number of high quality recordings have made it possible to determine the depth to 15 km, with an epicenter at 59.74°N and 5.38°E. Altogether 19 aftershocks were observed and the best ones were located (by master event technique) to within 1 km of each other. It is seen from Fig. VII.4.1 that this event is located to one of the most seismically active areas at the coast of Western Norway.

Using the nearest station with unsaturated data (BLS, Δ = 73 km), an analysis of source-displacement spectra (S-waves) gave a seismic moment of about $2 \cdot 10^{21}$ dynes-cm, but with no clear indication of corner frequency. It was quite clear, however, that very high Q-values (well above 1000) would be needed in the path correction time.

The source dimension was then obtained from the time between the P-wave onset to the first zero crossing following the method outlined by Frankel and Kanamori (1983). Two of the closest stations (BLS and SJD) were used, and assuming a circular fault, a source radius of 0.26 km was obtained. The best agreement between source radii calculated for BLS and SJD was obtained using the NW striking fault from the fault plane solution (see Fig. VII.5.1). A source radius of 0.26 km is comparable to the source dimension of the aftershock area. The stress drop was calculated to 50 bars using the Brune formulation and above values for moment and source radius.

The fault plane solution (Fig. VII.5.1), using first motions from 21 stations, shows a thrust fault with the compressional axis going nearly east-west. Lineation of aftershock epicenters indicates that the nodal plane striking N34°W and dipping 60° could be the fault plane, a solution which is in good compliance with the local faulting pattern in the area.

The two 1954 Stord events (M_b = 4.9) were relocated (59.82°N, 5.33°E) 10 km to the northwest of the 1983 event, and it seems that they could have been on

the same fault. This and the fault plane solution suggest that the active faults in this part of western Norway may follow the north-west striking system of fjords and not the geologically more dominant north-east striking Caledonian folding axis (see Fig. VII.5.2).

J. Havskov, Univ. of Bergen
H Bungum

References

Frankel and Kanamori (1983): Determination of rupture duration and stress drop for earthquakes in Southern California. Bull. Seism. Soc. Am., 1527-1551.

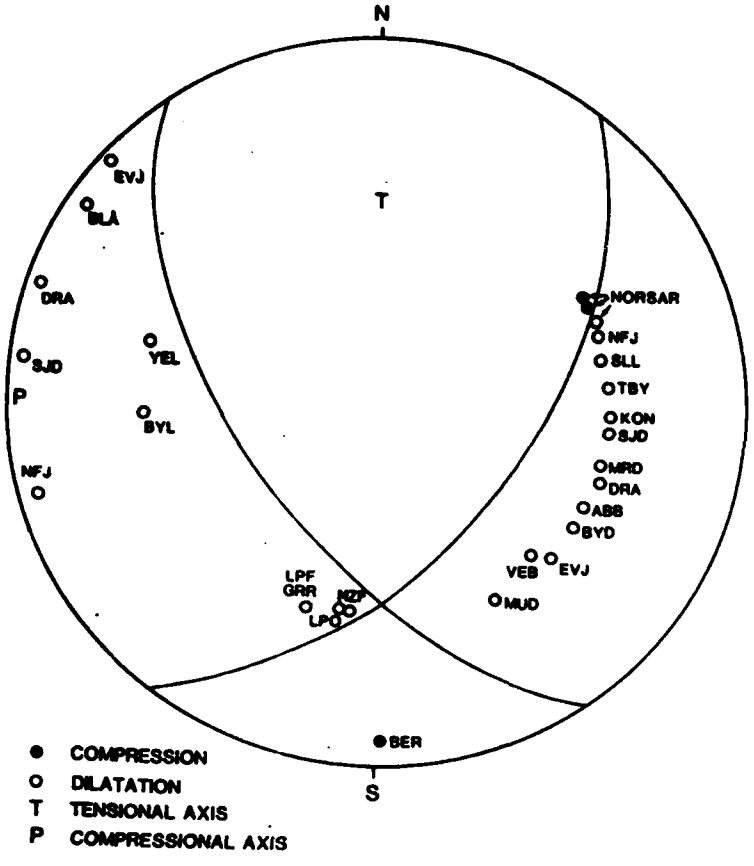

Fig. VII.5.1 Focal mechanism solution for the M_L=4.6 Stord earthquake on 8 March 1983.

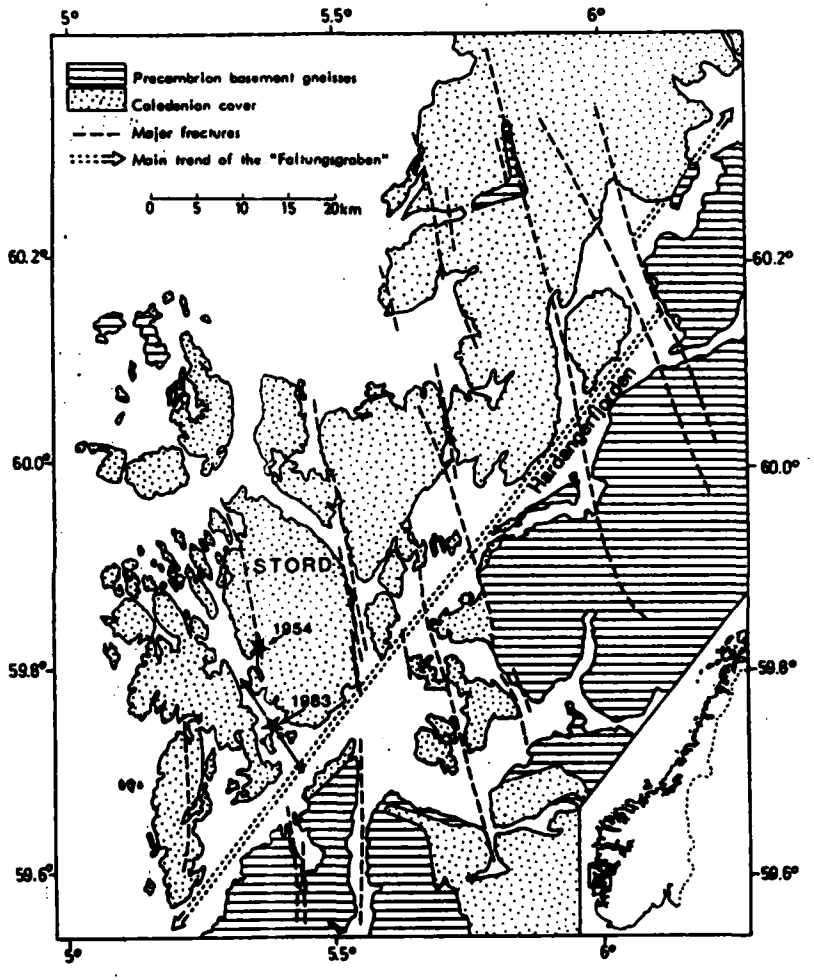

Fig. VII.5.2 Outline of geological features in the general Stord area. The location of the 1984 earthquake is indicated (with the most probable fault orientation) together with a relocalized m_b 4.9 earthquake from 7 July 1954.

VII.6 Report on an affordable, interactive and mobile seismic array installation

The primary objectives of seismic arrays are to monitor earthquake and nuclear explosion occurrence both on local and global scales, and to provide a data base for further research. However, large arrays such as NORSAR are costly to build and have high operational and maintenance overheads. On the other hand, technically simple arrays without an integrated time basis and non-digital recording produce data which are extremely difficult to handle and analyze efficiently. This article reports on the realization of a fully automated digital miniarray that is affordable for most research groups.

The basic concept here is that of the Remote Seismic Terminal Enhanced (RSTE), a field unit whose tasks comprise analog/digital conversion of data streams, real-time event detection processing, creation of event logs/seismic bulletins as a background processing task and finally temporary storage of original event data of significance.

The data center unit is operated by an RST which may be a much simpler device, say based on a personal computer with graphics installed in a study at home. The major tasks of the RST are to retrieve data from the field, download new operational instructions for the RSTE, redefine operational parameters, etc. The RST/RSTE communication link may either be via the switched telephone network, satellites or other convenient means.

The miniarray system we are now designing may be termed a second-generation RSTE/RST system, as our first generation, tied to a small North Star minicomputer, already has been demonstrated to work satisfactorily (e.g., see Husebye and Thoresen, 1984). Design considerations here are to:

- take advantage of recent improvements in communications systems and advances in microcomputer technology
- to produce a presumably affordable seismological recording system that can retrieve, process and transfer data in automated and semi-automated modes from an array remotely located

- to produce continuous/detected data from an unattended array that is immediately available to the user, thereby severing links with slow and cumbersome centralized data centers. Adding a color graphic display option to the host computer entails that waveform displays and associated analysis results can easily be visually assessed by the user even if the RST is based on a personal computer set-up.
- to produce a mobile and interactive system that allows the user ultimate flexibility in creating his own data base.

Present hardware configuration (Fig. VII.6.1)

The RSTE is based on the OMNIBYTE minicomputer which is powerful and consequently relatively expensive. Its choice was motivated by flexibility in software development for a prototype system. Adding a multiplexer to the A/D converter, it can handle up to 32 channels (differential inputs or 64 single-ended channels), although A/D conversion and multiplexing 8 channels of 16 bits requires 4 ms. We are considering a double input from each seismometer; one unfiltered and one analog bandpass filtered channel. The S-500 seismometer is inexpensive and completely portable without the need for a mass lock. It can be operated as either a vertical or horizontal instrument in a variety of environmental conditions. Peaked at 1 Hz, the instrument response is virtually flat to 100 Hz.

The RST is configured around a personal computer (PC-type, IBM compatible) with Polyforth operating system and language. Any reasonable computer may serve as host, although use of a PC is to emphasize the personal seismometry aspect. A color graphics option is included for waveform display enabling interactive operations thereby providing an analyst with considerable flexibility in seismogram analysis.

System design principles

Array operation as seen today or in the past comprises five major tasks, which naturally are incorporated into the remotely located miniarray. These tasks are:

i) Data transmission from seismometer to RSTE. In order to save on costly transmission fees charged by local telecommunications utilities, it is essential that data processing takes place in the field. A/D conversion is at the seismometer vault to cut down on transmission line noise.

ii) Real-time event detection processing. Noise suppression is via simple bandpass filtering. Detector design is by the relatively simple STA/LTA process operating on a 'voting' detector. It has been decided to abandon beamforming detection because of its extravagant computing requirements and in this context, negligible detection abilities over the voting detection scheme.

iii) Event analysis; signal parameter extraction and event log (daily bulletin preparation. This will be performed by the RSTE without any analyst intervention. Fast frequency-wavenumber analysis combined with phase/seismicity zone recognition algorithms ensures that bulletin preparation will include all quality data.

iv) External hardware testing and operational software modifications. In this system it is possible to down-load operational parameters (such as filter parameters, A/D converter gain settings, detector threshold levels, etc.) from the RST to the RSTE, and perform simple response tests of the seismometers.

v) Communication, data storage and exchange. This can be decided upon by the user and may be via switched telephone networks, radio/microwave telemetry, dedicated data links or satellite communications. It is estimated that only 5 mbyte of data are to be transferred daily, and will not be a costly operation.

The hardware/software system is schematically shown in Fig. VII.6.2 and is planned to be operational in August 1984.

Cost breakdown

The hardware cost for the compact RSTE field unit (excluding seismometers) consisting of CPU board, A/D converter, 4 mbyte RAM and modem is estimated

to roughly $6000, while an RST (personal computer, graphics monitor/software and modem) is estimated to roughly $4000.

E.S. Husebye
S.F. Ingate
E. Thoresen, Comtec A/S
J.A. Mathiesen, NTH, Trondheim

Reference

Husebye, E.S. and E. Thoresen (1984): Personal seismometery now! EOS, May 1984 (in press).

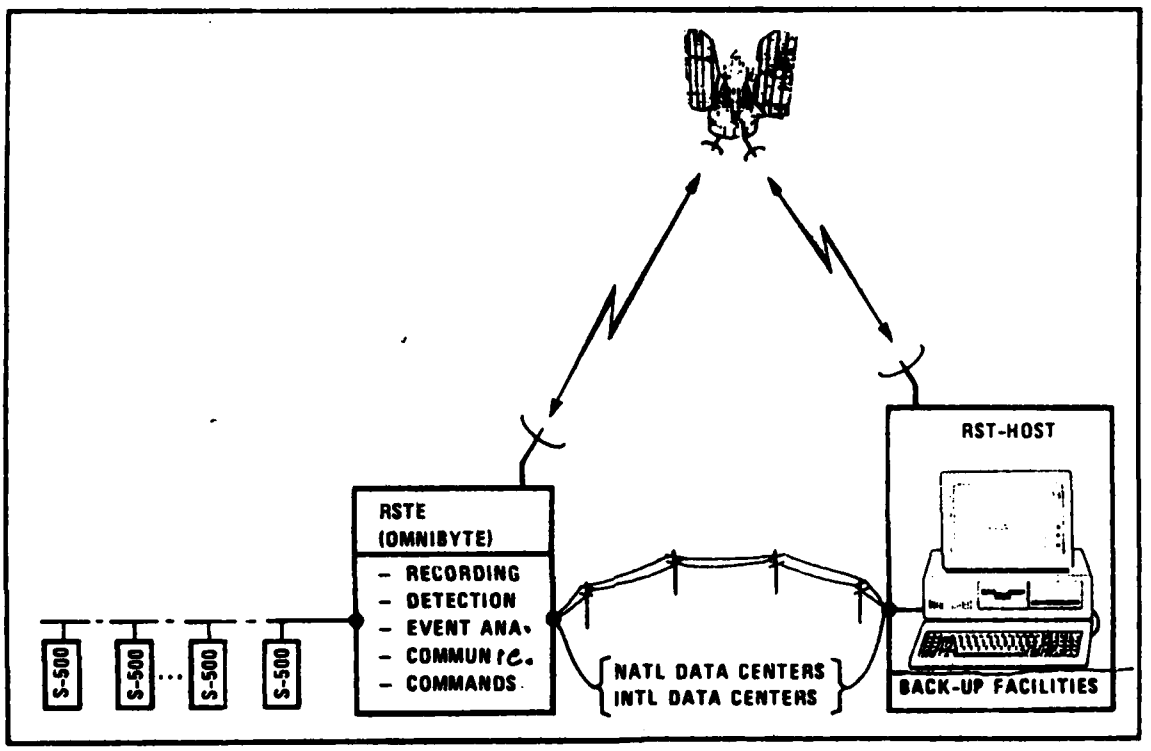

Fig. VII.6.1 Illustration of the RSTE/RST concept (Remote Seismic Terminal (Enhanced)). The RSTE is a specialized minicomputer system in the field whose main tasks are to sample, control and analyze outputs from an array of seismometers. It is remotely controlled, including options for software modifications, from an RST or host computer which ever may be of the 'personal computer' type. Back-up facilities may comprise a printer, and extra data storage on disk or tape. The only similarities between the RSTE and RST are the communications protocols for transfer of selected 'raw' data and analysis results from field to host, and down-loading commands in the RSTE system from the RST. National and international seismological data centers may be granted permission to independently extract data and/or analysis results from the RSTE or RST.

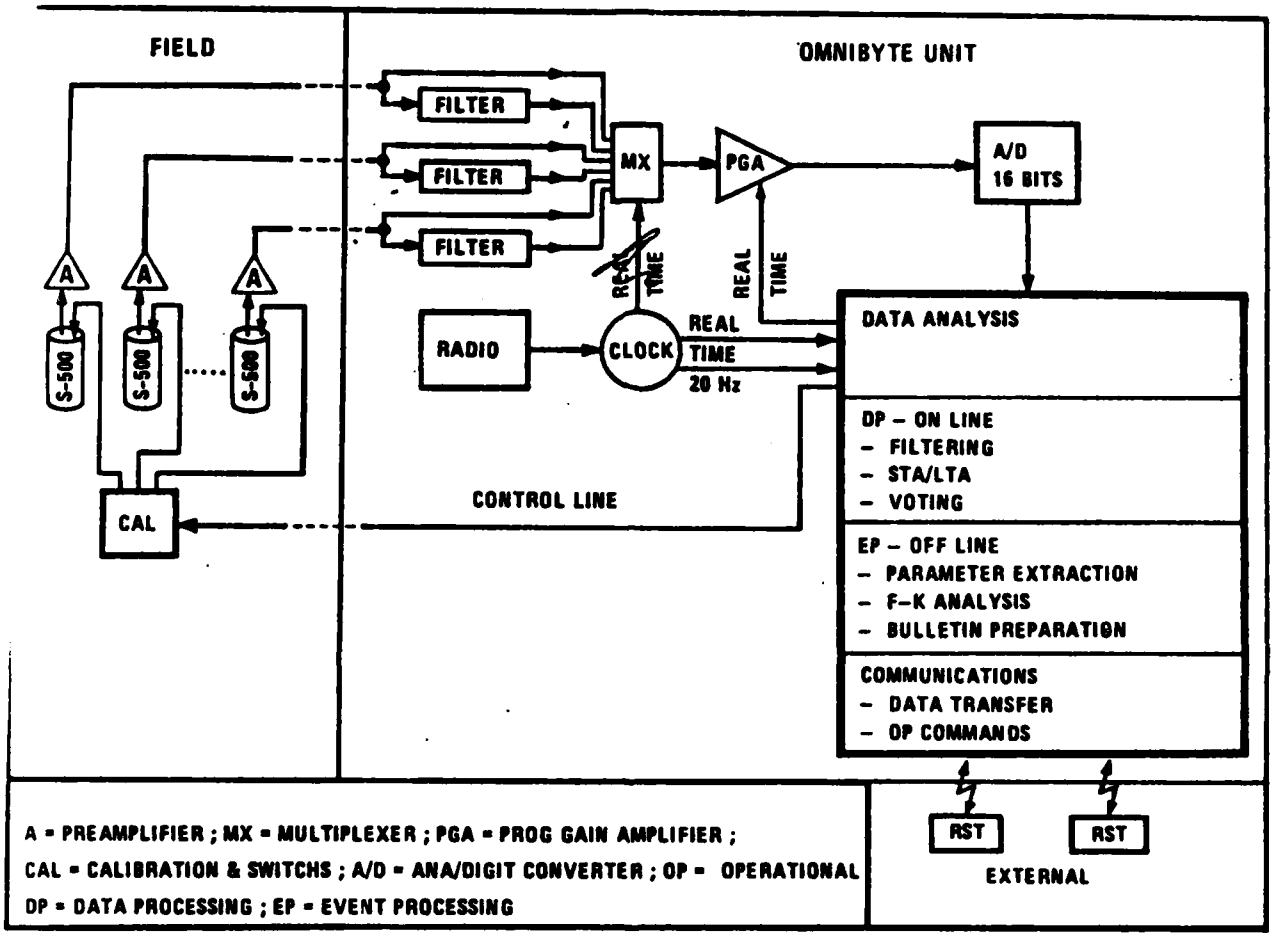

Fig. VII.6.2 The RSTE hardware configuration as detailed in text plus the essential steps involved in the data analysis centered on the powerful OMNIBYTE minicomputer. Using a multiplexer the A/D converter can handle up to 32 channels, which, if desired, permits seismometer inputs to be split in two, for example, an unfiltered and an analog-filtered channel. Such an option would reduce the CPU-load during the on-line detection processing.

VII.7 US ice-drift station FRAM IV: Preliminary analysis of multichannel seismic refraction data

The US ice-drift station FRAM IV was deployed in the Arctic Ocean on 15 March 1982 about 200 n.m. north of Svalbard and operated for 57 days during which the station drifted about 165 n.m. southwestwards from the Eurasian Basin onto the northern flank of the Yermak Plateau (Fig. VII.7.1). This was a multidisciplinary geophysical-geological expedition involving scientists from the US and Norway. A review of seismic operations in the Arctic has been given by Baggeroer and Duckworth (1983). Details of the Norwegian part of the field program per se and preliminary results from the rather extensive reflection surveys have been reported respectively by Kristoffersen (1982) and Kristoffersen and Husebye (1984).

A main component of the joint MIT/WHOI and Norwegian Polar Research Institute/ NORSAR program was acquisition of seven 20-30 km long lines of seismic 20 channel refraction data by dropping charges in open or newly refrozen leads less than 0.5 m thick, and detonated by depth sensitive primers set at 256 m depth. 55 lbs cans of TNT were used out to 40 km range and 110 lbs farther out. These shots were recorded on a linear array about 1.3 km long. This contribution outlines the initial phase of the refraction data analysis.

The DFS-V was started recording at the second minute mark after the reported charge drop time (average sinking time 2 mins 40 sec) and run for 100 seconds. A drum recorder was used as single channel monitor. The relatively long recording window proved necessary for safe recording of all shots due to deviations in estimated arrival time incurred for various reasons. However, the long records which require near 3 Megabyte of memory for the demultiplexing operation necessitated very special software action and full dedicated capabilities of the currently configured IBM 4331.

Further outstanding problems exist; upon inspection of the playouts, different shot parameters to those of MIT-logged parameters are obtained. In addition, the hydrophone response function is markedly different for many sensors in the array. Considerable editing of data was required. The

latter problem may be circumvented by bench-testing of the sensors before deployment.

A record section showing the filtered output of one hydrophone for Line 4 is given in Fig. VII.7.2. The most obvious arrivals are those of the water-wave and its multiple seabed-surface ice bounces. The amplitudes are considerably larger than the subsurface refracted arrivals in the trace-normalized section. Indeed, some of these arrivals have very low S/R. In order that some information be gleaned on the small amplitude arrivals, some form of array processing must be used.

Classical methods of array analysis such as beamforming and multichannel Wiener filtering are of little benefit due to the poor spatial-frequency response of linear arrays and the non-space stationarity of the hydrophone response functions. However, semblance (Taner and Koehler, 1969) is a fairly robust form of velocity spectra computation in these circumstances, and is the ratio of stacked trace energy to input energy

$$S_T = \frac{\sum_t s_T^2}{M \sum_t \sum_{i=1}^{M} f_{it(i)}^2}$$

where the i-th output of M channels at time t is f(i,t(i)), and the velocity stack over M sensors in which t(i) corresponds to a trajectory with a particular velocity is given by

$$s_T = \sum_{i=1}^{M} f_{i,t(i)}$$

Semblance may be described as a multichannel filter which measures the common signal power over the channels according to a specified lag pattern.

It has a possible range of 0 to 1 and is a measure of coherency which is independent of the joint power level of the traces.

By way of example, this analysis is applied to a narrow time window for shot 1 in Line 4 (Fig. VII.7.3). The data are dominated by the large amplitude water-wave, with indications of a faster arrival. Fig. VII.7.4 shows the contoured velocity spectra using the semblance measure for the data displaying power as a function of slowness and travel-time. The energy corresponding to the water-wave is obvious with a velocity of 1.45 km/s. Additional peaks in the spectra with velocities of 4.17 and 1.85 km/s indicate the success with which this measure is able to stack and display low-amplitude coherent energy. This analysis is continuing prior to τ-p inversion for the seven lines.

S.F. Ingate
E.S. Husebye
Y. Kristoffersen, Norw.
Polar Research Inst., Oslo

References

Baggeroer, A.B. and G.L. Duckworth (1983): Seismic exploration in the Arctic Ocean. The Leading Edge, 2, No. 10, 22-27.

Kristoffersen, Y. (1982): US ice drift station FRAM-IV: Report on the Norwegian field program. Norsk Polarinstitutt Rapportserie Nr. 11.

Kristoffersen, Y. and E.S. Husebye (1984): A pilot study for seismic exploration in the Arctic Ocean, manuscript in preparation.

Taner, M.T. and F. Koehler (1969): Velocity spectra-digital computer derivation and application of velocity function. Geophysics, 34, 859-881.

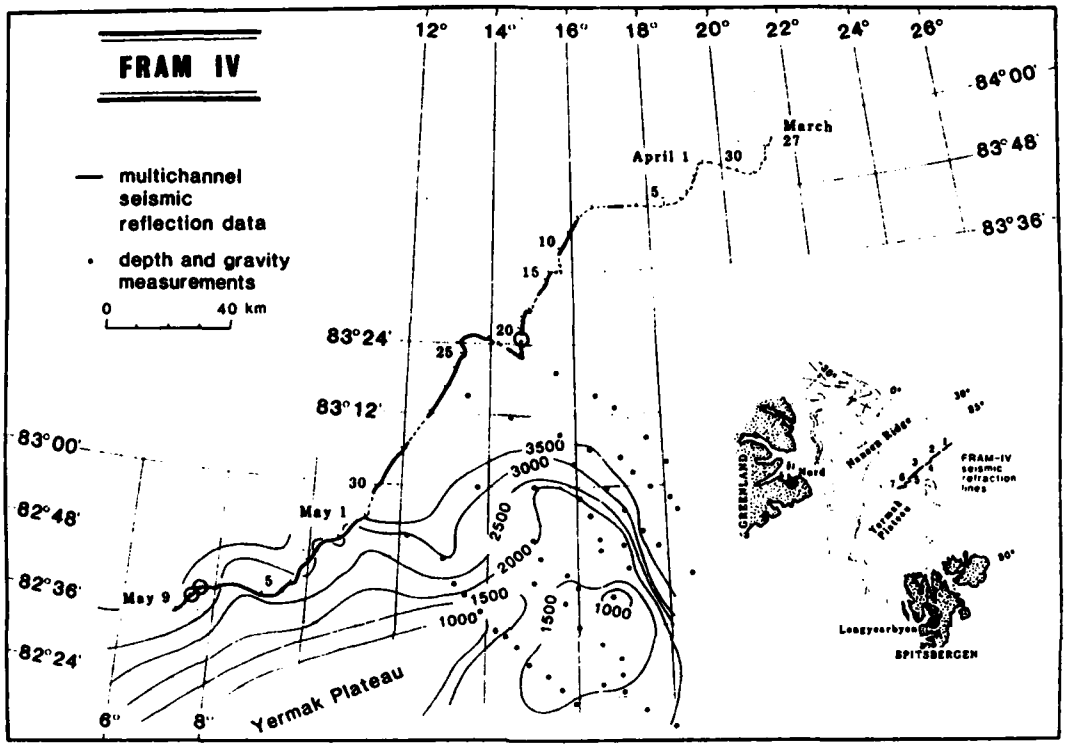

Fig. VII.7.1 Drift track of US ice drift station FRAM IV, March-May 1982, and location of refraction lines. Depth in meters.

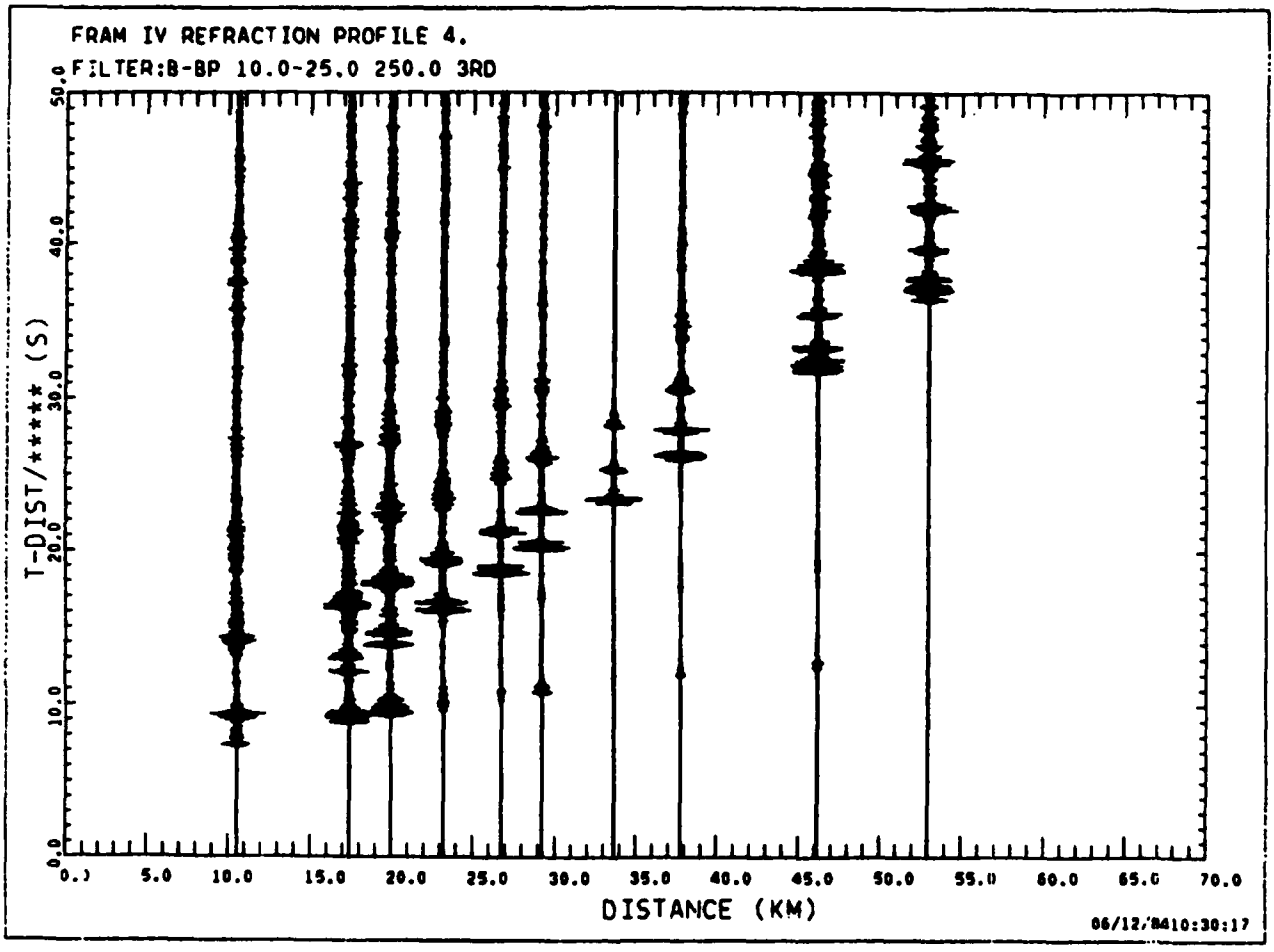

Fig. VII.7.2 Record section of filtered hydrophone playout for Line 4. Ten shots were recorded on 19th and 20th April 1982. Sampling rate in 4 ms. The dominant arrivals are the water-wave and multiple reflections.

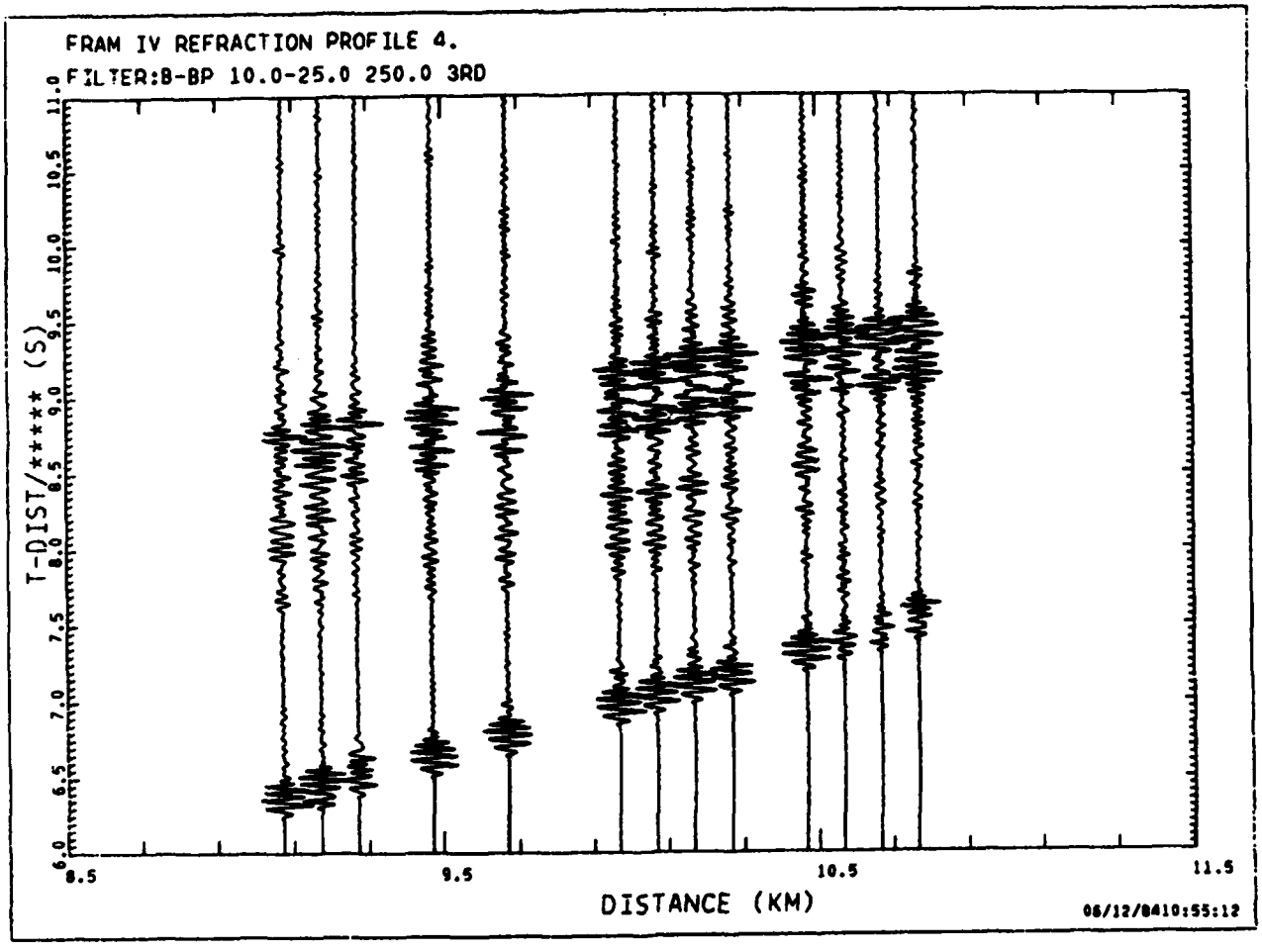

Fig. VII.7.3 Record section of filtered hydrophone playouts for a short time window, shot 1, line 4. Data have been edited for dead channels and polarity reversals of some channels. Note the large amplitudes of the direct water wave and its first multiple reflection, and the fast, low amplitude refracted arrival.

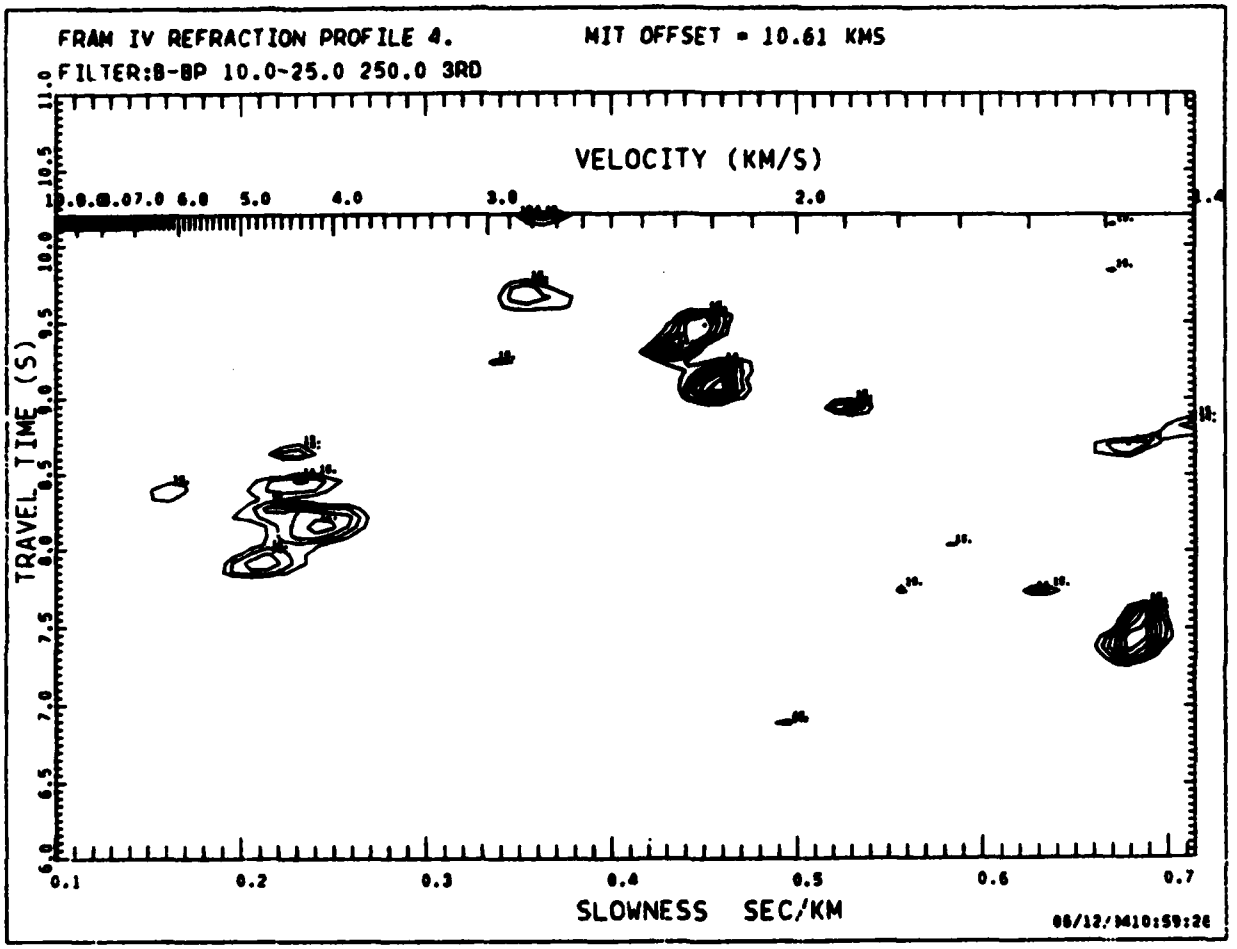

Fig. VII.7.4 Velocity spectra of the data in Fig. VII.7.3 using the semblance estimator. The direct water wave has a slowness of 0.69 s/km (vel. = 1.45 km/s), the first multiple of 0.47 s/km (2.12 km/s) and the refracted arrival of 0.26 s/km (3.85 km/s).

VII.8 The New Regional Array: 1983 Vertical and Three-Component Instrument Field Experiments

Introduction

During the period June 10 - July 5, 1983, data were recorded of a 5-element array of three-component instruments. The geometry of that array is shown in Fig. VII.8.1. During this period a number of local events were recorded.

The new array to be installed in 1984 will initially comprise 4 three-component instruments, whereof one will be located in a borehole at the center of the array. A proposal for location of the remaining 3 sets of three-component instruments is the purpose of the document.

Preliminary work

Before an analysis of the recorded three-component data can be conducted, it is important to reconsider the design of the 21-element vertical instrument regional array installed during the summer of 1983. The array configuration (Fig. VII.8.2) was based on an idealized analysis of the presumed noise field structure conducted by Mykkeltveit et al (1983) thereby enabling more than $\sqrt{N}$ (N = number of sensors) reduction in noise by simple beamforming. However, Husebye et al (1984) reported that there may be a coherent component in the noise field, thereby reducing the effective gain attainable by simple beamforming to be considerably less than $\sqrt{N}$. This has prompted reanalysis of the vertical component array data.

To examine the tenet proposed by Husebye et al, the experiment performed by Mykkeltveit et al is repeated here, i.e., computing correlation curves as a function of inter-sensor spacing and frequency, but with two innovations:

- During the period February - March 1984, the gain of each array element was raised by 12 dB. Effectively, this implies that the noise analysis can be conducted to a maximum frequency of 7 Hz before discretization levels are reached. This is in contrast to the upper limit in frequency of 4 Hz imposed on the Mykkeltveit et al experiment.
- A search for the coherent and/or propagating component in the noise field is possible by beaming the array to orthogonal directions (e.g., 0°

and 90°), and to 3 velocities, say ∞, 8 and 4.2 km/s. The latter two velocities approximately correspond to the phase velocities of Pn and Lg. In addition, cohrence along the edge of a presumed propagating noise wave front is examined by considering correlations between sensors aligned approximately parallel and normal to the wavefront.

Computational details

The data consists of 5 noise samples, each containing 100 seconds sampled at 40 Hz. The data are selected from different days spanning a full day. The data are bandpass filtered in the ranges 0.5-2.5, 1.5-3.5, 2.5-4.5, 4.0-6.0 and 6.0-8.0 Hz. Normalized correlations were computed between pairs of the 21 instruments giving 210 values and then averaged over the 5 samples and inter-sensor distance intervals of 150 meters. Some of the results are given in Fig. VII.8.3.

Results

The essential results of Mykkeltveit et al are replicated for beam velocities ∞ and 8 km/s (Fig. VII.8.3a, b); negative correlation values are observed for inter-sensor spacings in the range 200 meters to 1 kilometer, depending upon frequency.

However, no such results can be corroborated for a beam velocity of 4.2 km/s; the distance to where negative correlations exist varies with frequency (as expected) and beam direction. For example, at all frequencies higher than 3 Hz, negative correlations are consistently observed at inter-sensor distances of at least 100 m less for beam velocity 4.2 km/s than for ∞ or 8 km/s. For the beam direction 90°, correlations remain strongly positive even for large inter-sensor spacings at high frequencies (Fig. VII.8.3d). This implies that the noise is propagating with a reasonable degree of coherency from the east.

The second part of this exercise examines correlations between pairs of sensors parallel and normal to the presumed noise wavefront. Specifically, Fig. VII.8.3e,f examines instrument pairings aligned approximately parallel and normal to the

steering direction of 0°, respectively. Beam velocity is 4.2 km/s. It can be seen that for this particular beam, the correlations are much as expected for the case of non-propagating, incoherent isotropic noise. However, there are some differences, particularly at inter-sensor spacings of less than 300 meters. This may be due, in part, to leakage of coherent noise from the source to the east of the array. Fig. VII.8.3g,h examines instrument pairing aligned approximately normal and parallel to the steering direction of 90°, respectively. The strongly positive correlations at small inter-sensor spacings indicate that the noise wavefield is reasonably coherent both along the edge of the wavefront and in the direction of propagation from east to west. It is important to note that this is true for a wide range of frequencies, from 0.5 to 8 Hz, and so it is not simply noise propagating in a narrow pass-band. It is also likely that the source to the east of the array is non-transient, i.e., stationary, because of the wide time span sampled by the noise data.

The main conclusions to be drawn from this work are:

- A certain directability in the noise field is apparent for certain azimuth directions. In practice this gives reduced noise suppression capabilities or an equivalent higher false alarm rate on certain beams.
- Array configuration optimization; this is a problem if reasonable performance is desired over a relatively wide frequency range. Optimum processing schemes (Husebye et al, 1984) appear to be unavoidable here or the array must compromise on a duality in configuration.

Analysis of three-component data

The data consist of 5 noise samples, each containing 100 seconds recorded by the 5 three-component sets in the preliminary NORESS array. As before, the data are selected from different days spanning a full day. The data are bandpass filtered in the ranges 0.5-2.5, 1.5-3.5 and 2.5-4.5 Hz. Correlations were computed between pairs of the orthogonal components, and then averaged over the 5 samples. Standard deviations of correlation were larger for this exercise than for the vertical instrument array, because no averaging over inter-sensor spacing intervals was possible. This is reflected in the correlation plots (Fig. VII.8.4) where the curves appear quite jagged due possibly to incorrectly matched instrument responses.

Correlation curves for three components with beam velocities ∞ and 8 km/s (two steering directions, 0° and 90°) are shown in Fig. VII.8.4a,b,c. The curves exhibit the general properties for isotropic noise, as found in the preliminary work using the vertical instrument array. Fig. VII.8.4d,e shows the results for the beam velocity of 4.2 km/s. The poor correlations for beam direction 0°, particularly in the higher frequency pass-band of 2.5-4.5 Hz, show that the noise is largely incoherent. For the beam direction 90°, the noise exhibits a greater degree of coherence. This again indicates that there is a probable source of stationary noise to the east of the array.

Recommendations for deployment of three-component instruments

With one three-component instrument centrally located in the array, deployment of the three remaining instrument sets in the C-ring, specifically at site numbers 1, 12, 14 and 16 is advised. The minimum inter-sensor spacing for instruments deployed this way is about 700 meters which is perhaps the best compromise based on the noise correlation curves in this study and signal correlation curves from Mykkeltveit et al. Average inter-sensor spacings for instruments placed in the B-ring are 300 meters, and for the D-ring, 1500 meters. Clearly, however, much denser station spacing is required. It is imperative that an additional 3 or 4 sets of three-component instruments be considered for deployment in summer 1984.

The usefulness of an array of three-component instruments in detection and location modes has yet to be examined. Future areas of study include the use of sophisticated multivariate schemes such as principal-component analysis (of which polarization and particle motion studies are a subset). However, the initial deployment of only 4 three-component instruments will not create a sufficiently large data base for such studies, as can be seen from the considerable scatter in the correlation estimates of Fig. VII.8.4. Nevertheless, four sets of instruments will be useful for determining preliminary directions of future research.

S.F. Ingate

References

Husebye, E.S., S.F. Ingate and A. Christoffersson (1984): Optimum processing schemes in real-time analysis of array data, in Technical Means of Verification of Compliance with Arms Control Agreements (in press).

Mykkeltveit, S., K. Åstebøl, D.J. Doornbos and E.S. Husebye (1983): Seismic array configuration optimization. Bull. Seism. Soc. Am., 73, 173-186.

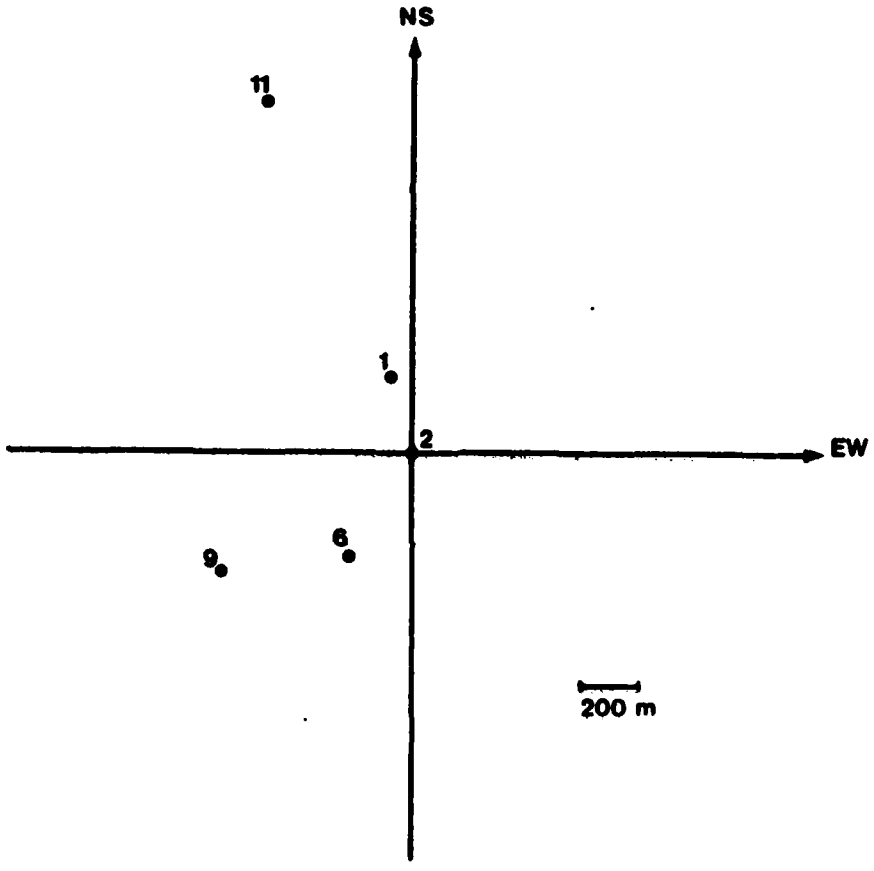

Fig. VII.8.1 Temporary 5-element, three-component short period seismometer experimental array, deployed June 10 - July 5, 1983.

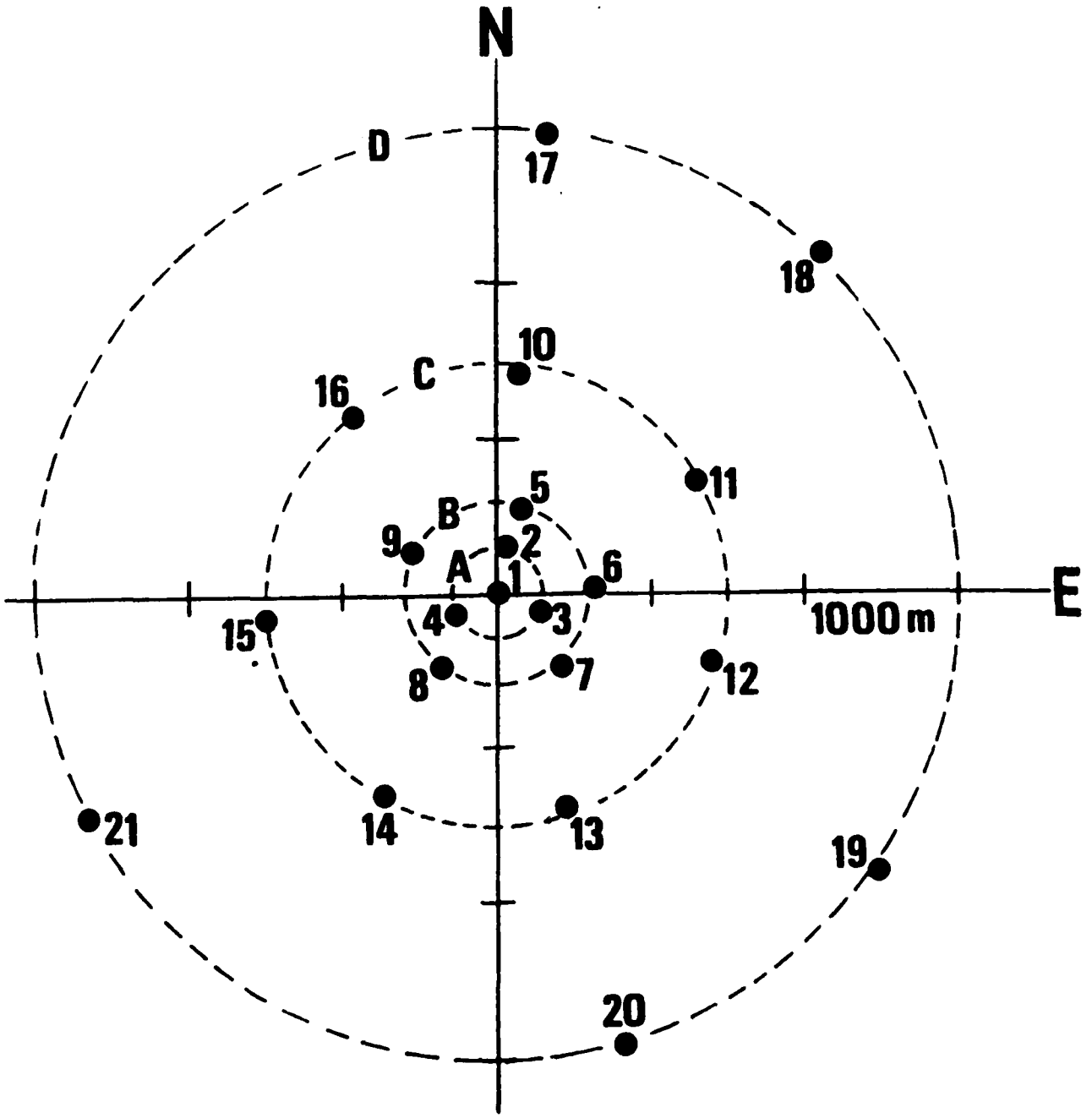

Fig. VII.8.2 The prototype 21-element vertical component short period seismometer array, with site numbering. Deployed summer 1983 to present.

Fig. VII.8.3 Correlation versus inter-sensor spacing for noise recorded on the prototype regional array. Five frequency bands are shown, 1 (0.5-2.5 Hz), 2 (1.5-3.5 Hz), 3 (2.5-4.5 Hz), 4 (4.0-6.0 Hz) and 5 (6.0-8.0 Hz). Each curve is based on measurements from 210 combinations of sensor pairs.
(a) Beam velocity = ∞ km/s.
(b) Beam velocity, direction = 8 km/s, 0°.
(c) Beam velocity, direction = 4.2 km/s, 0°.
(d) Beam velocity, direction = 4.2 km/s, 90°.
(e) Beam velocity, direction, alignment = 4.2 km/s, 0°, parallel to wavefront
(f) Beam velocity, direction, alignment = 4.2 km/s, 0°, normal to wavefront.
(g) Beam velocity, direction, alignment = 4.2 km/s, 90°, normal to wavefront.
(h) Beam velocity, direction, alignment = 4.2 km/s, 90°, parallel to wavefront.

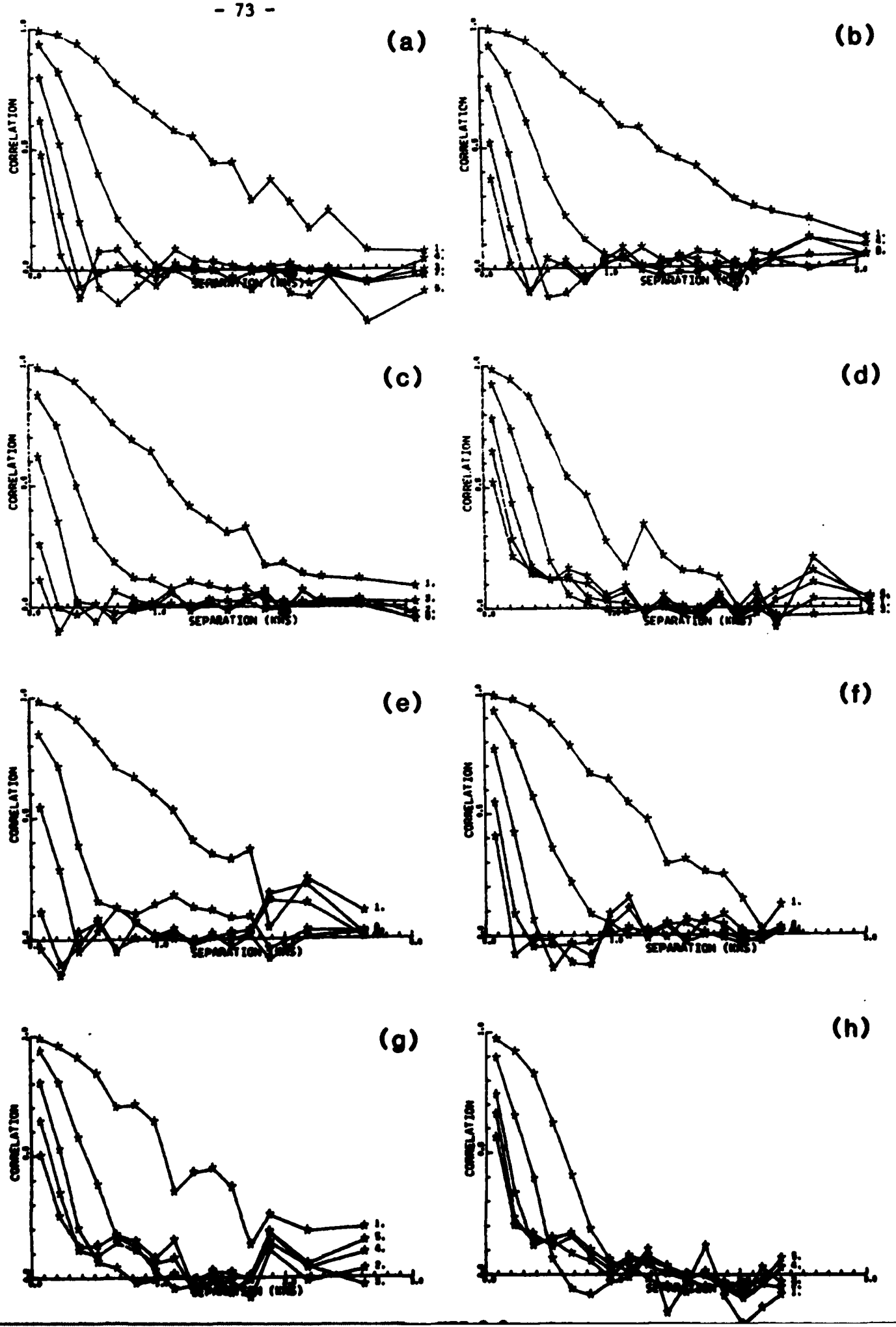
(a)
(b)
(c)
(d)
(e)
(f)
(g)
(h)
CORRELATION
SEPARATION (KMS)

Fig. VII.8.4 Correlation versus inter-sensor spacing for noise recorded on the temporary three-component seismometer array. Three frequency bands are shown, 1 (0.5-2.5 Hz), 2 (1.5-3.5 Hz) and 3 (2.5-4.5 Hz).
(a) Beam velocity = ∞ km/s.
(b) Beam velocity, direction = 8 km/s, 0°.
(c) Beam velocity, direction = 8 km/s, 90°.
(d) Beam velocity, direction = 4.2 km/s, 0°.
(e) Beam velocity, direction = 4.2 km/s, 90°.

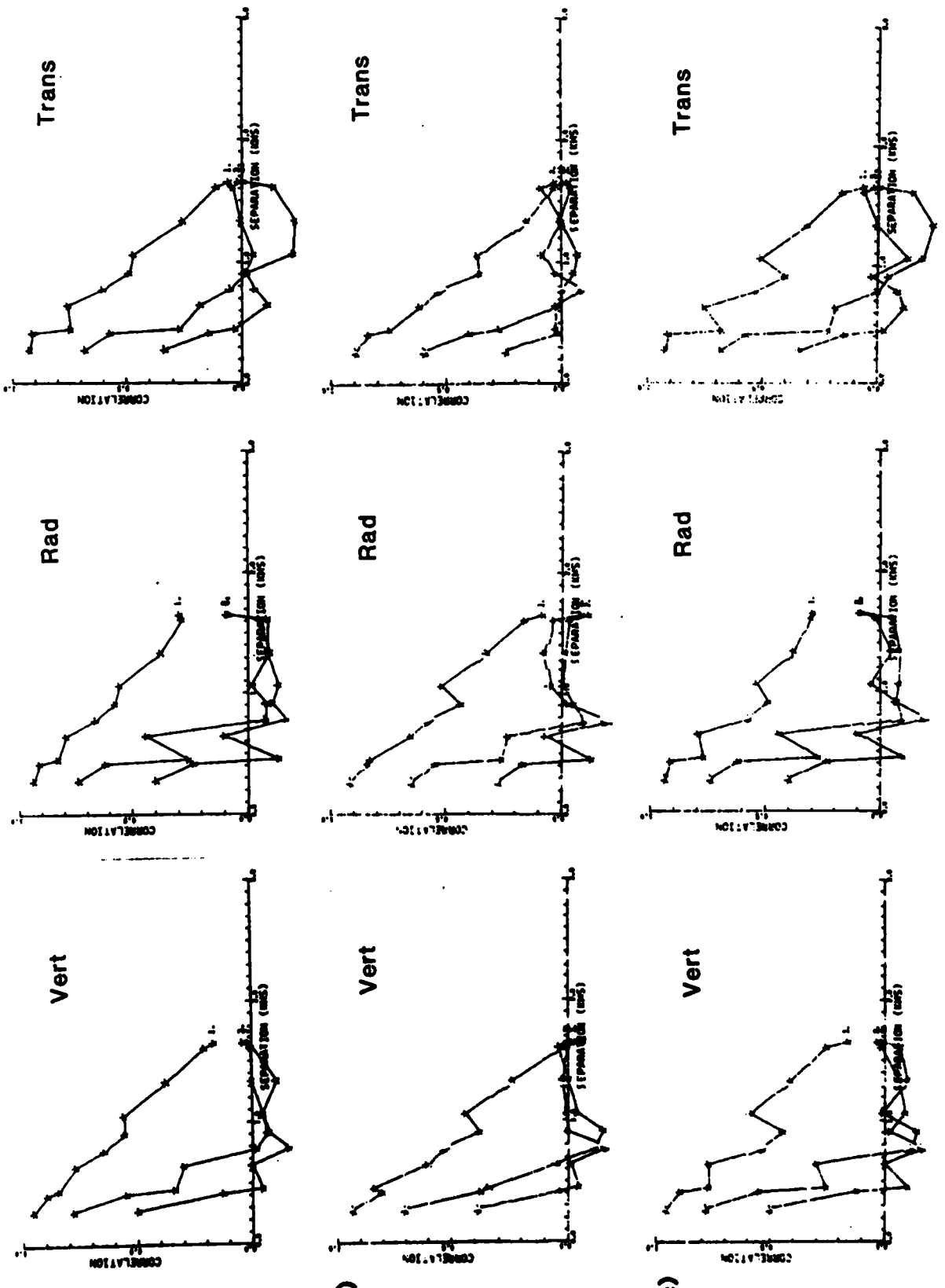

Fig. VII.8.4

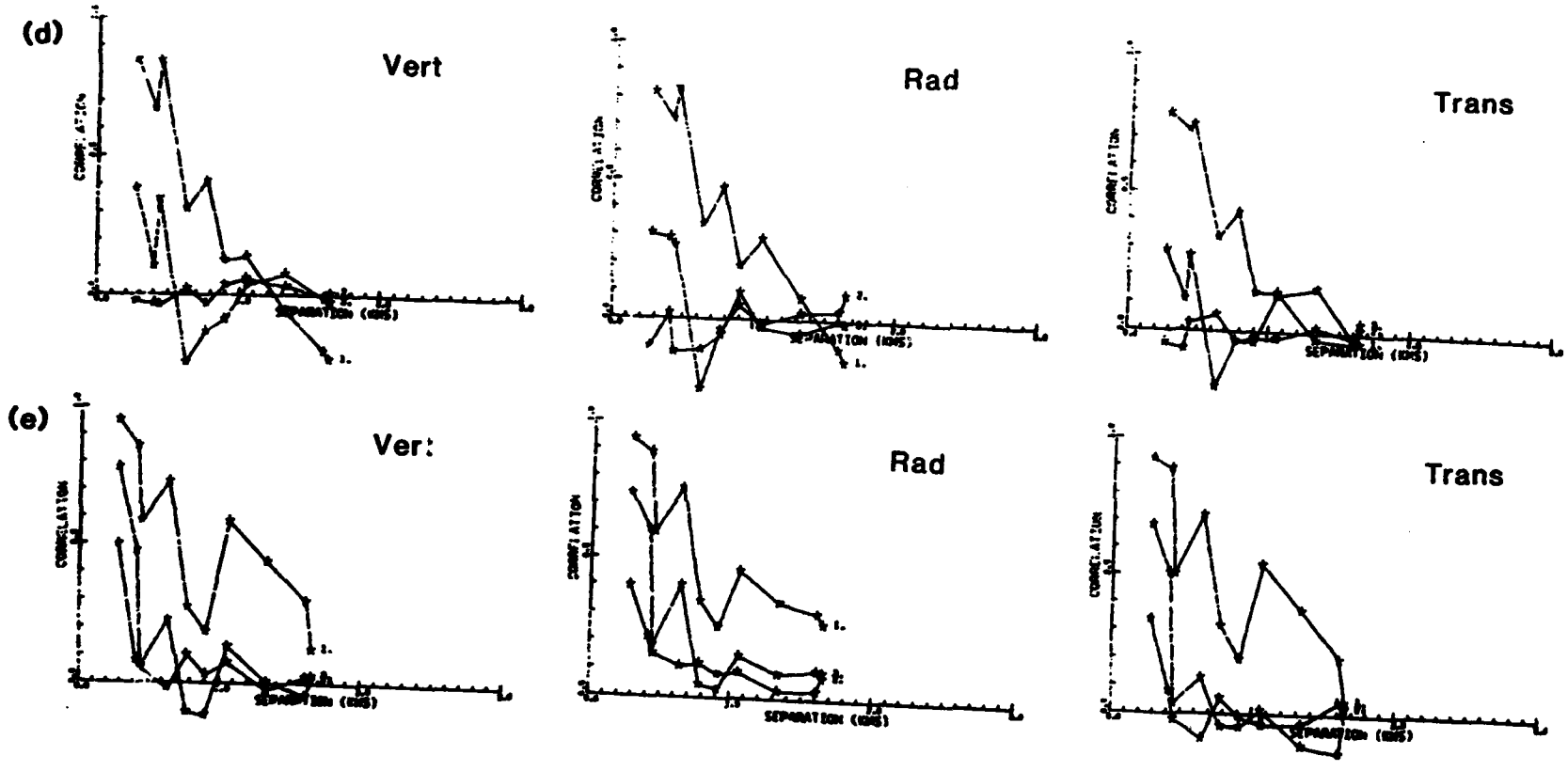

Fig. VII.8.4 (cont.)